J. Fluid Mech. (2004), *vol.* 517, *pp.* 281–308. © 2004 Cambridge University Press
DOI: 10.1017/S0022112004000977 Printed in the United Kingdom

Stratified turbulence dominated by vortical motion

By MICHAEL L. WAITE AND PETER BARTELLO

McGill University, 805 rue Sherbrooke ouest, Montréal, QC H3A 2K6, Canada
michael.waite@mail.mcgill.ca

(Received 21 November 2003 and in revised form 26 May 2004)

We present numerical simulations of stably stratified, vortically forced turbulence at a wide range of Froude numbers. Large-scale vortical forcing was chosen to represent geophysical vortices which break down at small scales where Coriolis effects are weak. The resulting vortical energy spectra are much steeper in the horizontal direction and shallower in the vertical than typical observations in the atmosphere and ocean, as noted in previous studies. We interpret these spectra in terms of the vertical decoupling which emerges in the strongly stratified limit. We show that this decoupling breaks down at a vertical scale of U/N, where N is the Brunt–Väisälä frequency and U is a characteristic horizontal velocity, confirming previous scaling arguments. The transfer of vortical energy to wave energy is most efficient at this vertical scale; vertical spectra of wave energy are correspondingly peaked at small scales, as observed in past work. The equilibrium statistical mechanics of the inviscid unforced truncated problem qualitatively predicts the nature of the forced–dissipative solutions, and confirms the lack of an inverse cascade of vortical energy.

1. Introduction

Stable stratification is ubiquitous in geophysical and astrophysical fluids (for reviews see Hopfinger 1987; Riley & Lelong 2000). Stratification inhibits vertical velocity, causing the collapse of isotropic turbulence into layered, quasi-horizontal motion with strong vertical variability. Internal gravity waves are superimposed on this layered flow, which is described as the vortical or 'pancake' component of the turbulence. In the atmosphere and ocean, stratification and rotation are both important at large scales, and the flow is predominantly vortical (quasi-geostrophic). As one moves downscale into the atmospheric mesoscale and oceanic submesoscale, Coriolis effects weaken and stratification dominates. In this study, we examine the breakdown of vortical motion in stratified turbulence in the absence of rotation.

In the atmospheric mesoscale and the oceanic submesoscale, vortical motion has been observed to coexist with internal waves (see Cho, Newell & Barrick 1999 for the atmosphere, and Polzin *et al.* 2003 for the ocean). Significant progress has been made on the problem of weakly nonlinear internal waves, which emerge in the limit of strong stratification (e.g. McComas & Müller 1981; Müller *et al.* 1986; Caillol & Zeitlin 2000). However, the study of internal waves has so far tended to neglect the effects of vortical motion. This neglect is problematic, since Lelong & Riley (1991) showed that vortical motion can affect wave evolution in two ways: by facilitating the transfer of energy between waves, and by exchanging energy with the wave field (see also Godeferd & Cambon 1994; Bartello 1995; Babin *et al.* 1997; Embid & Majda

https://doi.org/10.1017/S0022112004000977 Published online by Cambridge University Press

1998). Vortical motion coexists with and modifies the wave field, and so a thorough understanding of its dynamics is necessary.

Compared with internal waves, much less progress has been made on the problem of vortical motion. In the limit of strong stratification, vortical motion is governed by a reduced set of equations, which describe layers of horizontal, non-divergent and fully nonlinear motion coupled only by viscosity (Riley, Metcalfe & Weissman 1981; Lilly 1983; Babin *et al.* 1997; Embid & Majda 1998). Similarities between the reduced equations and two-dimensional turbulence have provoked speculation that stratified turbulence might support an inverse cascade of energy as in two dimensions (Gage 1979; Lilly 1983). However, attempts to generate an inverse cascade in numerical simulations of stratified turbulence have been unsuccessful, probably due to the strong dissipation between layers, and a loss of vortical energy into internal waves and small-scale turbulence (Herring & Métais 1989; Métais *et al.* 1996). Godeferd & Cambon (1994) used the eddy-damped quasi-normal Markovian (EDQNM) closure to show that the vortical mode dynamics act to transfer energy in spectral space towards the vertical wavenumber axis, corresponding to strong layering. Both layering and flat pancake-shaped vortices have been observed in numerical simulations (e.g. Herring & Métais 1989; Kimura & Herring 1996; Godeferd & Staquet 2003; Riley & deBruynKops 2003) as well as laboratory experiments (e.g. Thoroddsen & Atta 1992; Fincham, Maxworthy & Spedding 1996; Billant & Chomaz 2000). The layering of vortical motion generates vertical shear which, if sufficiently strong, causes the flow to break down into overturning density surfaces and small-scale turbulence. The overturning scale (the largest vertical scale at which overturning occurs) thus sets the thickness of the layers. The dynamical distinction between vortical and wave motion is lost at and below the overturning scale.

Observations in the atmosphere and ocean have motivated a number of theories of stratified turbulence. In the atmospheric mesoscale, horizontal wavenumber spectra are frequently found to have the form $k_h^{-5/3}$ for length scales of $O(1)$–$O(1000)$ km (Nastrom & Gage 1985). Vertical wavenumber spectra of the form k_z^{-3} are often reported (Smith, Fritts & Van Zandt 1987). In fact, deviations from these 'universal' forms are commonly observed: horizontal spectral slopes near -3 for scales smaller than a few kilometres (Bacmeister *et al.* 1996), and vertical spectral slopes between -2 and -3 (e.g. Nastrom, Van Zandt & Warnock 1997). In the ocean, vertical wavenumber spectra vary as k_z^{-2} at scales larger than 10 m, steepening to k_z^{-3} at smaller scales and then shallowing to $k_z^{-5/3}$ at even smaller scales (e.g. Gargett *et al.* 1981). Early theories for these spectra were based on dimensional analysis. Bolgiano (1959) took the dissipation rate of mean-squared buoyancy fluctuations as an important parameter, and derived an isotropic energy spectrum proportional to $k^{-11/5}$. Lumley (1964) modified Kolmogorov's (1941) theory by accounting for the drain of kinetic to potential energy, and derived an isotropic spectrum of the form $E(k) \sim N^2 k^{-3}$ for $k \ll k_b$, where k_b is the buoyancy or Ozmidov wavenumber

$$k_b = \left(\frac{N^3}{\epsilon}\right)^{1/2}, \tag{1.1}$$

ϵ is the kinetic energy dissipation rate and N is the Brunt–Väisälä frequency. This theory predicts a transition to a Kolmogorov inertial range with $E(k) \sim \epsilon^{2/3} k^{-5/3}$ when $k \gg k_b$. The ratio of k_b to the Kolmogorov wavenumber

$$k_d = \left(\frac{\epsilon}{\nu^3}\right)^{1/4} \tag{1.2}$$

https://doi.org/10.1017/S0022112004000977 Published online by Cambridge University Press

(ν is the kinematic viscosity) determines whether small-scale isotropic turbulence occurs. Observations in the ocean indicate a well-resolved Kolmogorov inertial range between k_b and k_d when $k_d/k_b \gtrsim 1000$ (Gargett, Osborn & Nasmyth 1984). On the other hand, laboratory experiments by Fincham *et al.* (1996) and numerical simulations by Godeferd & Staquet (2003) had smaller values of k_b/k_d and anisotropic motion at the dissipation scale.

Early attempts to explain the atmospheric mesoscale spectrum highlighted the distinction between vortical and wave motion. Gage (1979) and Lilly (1983) suggested that the $k_h^{-5/3}$ spectrum might be due to an inverse cascade of vortical energy, while others including Dewan (1979) and Van Zandt (1982) argued that it could result from a forward cascade of internal wave energy. The observed vertical wavenumber spectrum in the atmosphere, on the other hand, is generally attributed to internal wave dynamics rather than vortical motion. Vertically propagating gravity waves grow in amplitude with height and 'saturate' when the growth is balanced by breaking and dissipation. Different saturation mechanisms, including convective and shear instabilities (Dewan & Good 1986; Smith *et al.* 1987) and Doppler spreading of small waves by large waves (Hines 1996), imply a vertical wavenumber spectrum with a tail of the form

$$E_z(k_z) \sim N^2 k_z^{-3}, \tag{1.3}$$

the so-called 'saturation spectrum'. The attribution of the observed vertical spectrum to wave processes raises the question of what spectrum is generated by vortical motion. The wave saturation theories, for obvious reasons, should not apply to flows dominated by vortical motion. Nevertheless, there seems to be a certain degree of anticipation in the literature that such flows should produce a spectrum of the form k_z^{-3} (e.g. Herring & Métais 1989; Billant & Chomaz 2001).

In addition to its spectrum, a key question about the vortical component of motion is how its vertical scale varies with stratification. Billant & Chomaz (2001) showed that in the limit of strong stratification, the inviscid Boussinesq equations are self-similar with respect to the variable zN/U, suggesting a characteristic vertical length scale of U/N, where U is a horizontal velocity scale and z is the vertical coordinate. The implication is that the vertical Froude number Fr_z remains $O(1)$ even as the horizontal Froude number Fr_h goes to zero, where

$$Fr_z = \frac{U}{NL_z}, \quad Fr_h = \frac{U}{NL_h}, \tag{1.4a,b}$$

and L_z and L_h are vertical and horizontal length scales. Like Dewan & Good (1986), Billant & Chomaz (2001) further assumed their scaling to hold at every vertical scale, identifying $L_z \sim 1/k_z$ and letting $U^2 \sim E(k_z)\,k_z$, from which the spectrum (1.3) follows. This is the only argument of which we are aware that predicts (1.3) for stratified turbulence dominated by vortical motion. Previous studies have suggested that U/N (with U defined as the root mean square (r.m.s.) horizontal velocity) is the vertical scale separating large-scale weakly nonlinear internal waves from small-scale strongly nonlinear waves and stratified turbulence (Munk 1981; Hines 1996).

Numerical simulations of stratified turbulence have had mixed success in reproducing the observed spectra. In flows dominated by vortical motion, spectra have been found to be steeper than $-5/3$ in the horizontal direction, and shallower than -3 in the vertical. Laval, McWilliams & Dubrulle (2003) found steep k_h spectra (with slopes near -5) and very shallow k_z spectra when large-scale vortical energy was forced. Wave energy, which was not forced directly, was peaked at small scales.

https://doi.org/10.1017/S0022112004000977 Published online by Cambridge University Press

On the other hand, Riley & deBruynKops (2003) and Lindborg (2003, personal communication) found k_h spectra consistent with a slope of $-5/3$. Lindborg (personal communication, 2003) also noted very shallow k_z spectra with sufficiently strong stratification. Simulations of internal wave breaking have had greater success in reproducing the observed $N^2 k_z^{-3}$ spectrum (Bouruet-Aubertot, Sommeria & Staquet 1996; Carnevale, Briscolini & Orlandi 2001). These studies of wave breaking confirmed the earlier results of Ramsden & Holloway (1992), who found a positive buoyancy flux (corresponding to the transfer of kinetic to potential energy, or restratification) at small scales, contrary to the premise of Lumley's (1964) theory.

In forced simulations of stratified turbulence in a periodic domain, a slow transfer of energy into the horizontally averaged flow (modes with $k_h = 0$) has been observed (Smith & Waleffe 2002; Laval *et al.* 2003). These modes are not permitted in domains with sidewalls such as the oceans; the question of whether their growth represents an under-resolved transfer to large but finite scales is still open. The mechanism of the transfer is thought to be either off-resonant or higher-order resonant interactions, since resonant triads cannot move energy into modes with $k_h = 0$ (Smith & Waleffe 2002). The long time scale of the growth makes it difficult to define statistical stationarity in forced simulations. Indeed, a choice must be made: run the simulations until the $k_h = 0$ energy saturates (can be prohibitively long); stop the simulations before significant growth occurs (can be too short to be useful); or finally, run the simulations for an intermediate duration, on the assumption that the systematic growth does not affect other quantities of interest. We have opted for the third choice.

In the work presented here, we use numerical simulations to study stratified turbulence dominated by vortical motion. We have chosen to perform forced simulations, which allow for the averaging of quantities at statistical stationarity, where a constant Froude number can be maintained. Some of the questions we have attempted to answer are: Do such flows produce spectra which are consistent with observations? At what scale does vortical motion break down into overturning? How effectively is wave energy generated by vortical motion? We have examined a wide range of stratifications, varying Fr_h between $O(1)$ and $O(10^{-2})$. The paper is organized as follows. In § 2, we recall the governing equations for a stably stratified fluid, as well as the normal mode decomposition of the flow into vortical and wave parts. In § 3, we examine the statistical mechanical equilibrium for truncated, inviscid stratified turbulence, and comment on the implications for the forced–dissipative problem and a possible inverse cascade of vortical energy. Section 4 contains the results of our simulations of stratified turbulence subject to large-scale forcing of vortical motion. We first consider a simulation of the reduced equations of strongly stratified turbulence, and then discuss our simulations of the full equations of motion at different stratifications. Conclusions are given in § 5.

2. Governing equations and normal mode decomposition

The three-dimensional equations of motion for a stably stratified fluid subject to the Boussinesq approximation are

$$\frac{\partial \boldsymbol{u}}{\partial t} + \boldsymbol{u} \cdot \nabla \boldsymbol{u} = -\nabla p + b' \hat{\boldsymbol{z}} + \boldsymbol{F} + D_u(\boldsymbol{u}), \tag{2.1a}$$

$$\nabla \cdot \boldsymbol{u} = 0, \tag{2.1b}$$

$$\frac{\partial b'}{\partial t} + \boldsymbol{u} \cdot \nabla b' + N^2 w = D_b(b'). \tag{2.1c}$$

https://doi.org/10.1017/S0022112004000977 Published online by Cambridge University Press

In (2.1), $\boldsymbol{u} = u\hat{\boldsymbol{x}} + v\hat{\boldsymbol{y}} + w\hat{\boldsymbol{z}}$ is the velocity; b' is the buoyancy, given by either $g\theta'/\theta_0$ or $-g\rho'/\rho_0$, where θ' and ρ' are potential temperature and density perturbations; θ_0 and ρ_0 are constant reference values; and p is the dynamic pressure divided by ρ_0. The Brunt–Väisälä frequency N is assumed to be constant. D_u and D_b are dissipation operators of velocity and buoyancy, and $\boldsymbol{F}$ is a velocity forcing function. We will make frequent use of Fourier-transformed variables in this paper, denoting the transform of a quantity $q(\boldsymbol{x}, t)$ by $\hat{q}_{\boldsymbol{k}}(t)$, where $\boldsymbol{k} = (k_x, k_y, k_z)$. Horizontal and three-dimensional wavenumbers are given by $k_h = (k_x^2 + k_y^2)^{1/2}$ and $k = (k_x^2 + k_y^2 + k_z^2)^{1/2}$. All variables are assumed to be triply periodic in a domain of size L^3.

Vortical and wave motions can be distinguished by their time scales as well as by potential vorticity (PV). The vortical time scale $T_v = L_h/U$ is traditionally given by the horizontal shear of the horizontal flow, while the wave time scale $T_w \sim 1/\sigma_k$ is defined by the dispersion relation

$$\sigma_k = \frac{Nk_h}{k}. \tag{2.2}$$

The ratio of time scales T_w/T_v is equal to Fr_h for the fastest waves. Nevertheless, even when $Fr_h \ll 1$ there are low-frequency wave modes near the k_z-axis with periods close to the vortical time scale. In terms of PV, we follow Lelong & Riley (1991) and define the vortical part of the velocity to be that which contributes to the PV, while the wave part is defined to have no PV. For the Boussinesq equations, the PV is given by Π/ρ_0, where

$$\Pi = \boldsymbol{\omega} \cdot (N^2\hat{\boldsymbol{z}} + \nabla b'), \tag{2.3}$$

and $\boldsymbol{\omega} = \nabla \times \boldsymbol{u}$. When $\boldsymbol{F} = 0$ and $D_b = D_u = 0$, Π satisfies

$$\frac{\mathrm{d}\Pi}{\mathrm{d}t} = 0 \tag{2.4}$$

(e.g. Pedlosky 1987). From (2.4), it is clear that for an inviscid unforced flow, vortical motion cannot be generated if none is present initially. Waves, on the other hand, can be created by vortical motion without violating PV conservation (e.g. Herring & Métais 1989; Lelong & Riley 1991; Bartello 1995).

In the absence of overturning, Π can be inverted for the vortical component of the flow (Staquet & Riley 1989). More commonly, a linear decomposition such as Craya–Herring (e.g. Herring 1974) or linear normal modes (Godeferd & Cambon 1994; Bartello 1995) is used. We employ the linear normal mode decomposition of (2.1), which we will briefly review. Following Bartello (1995), the Fourier-transformed variables $(\hat{\boldsymbol{u}}_{\boldsymbol{k}}, \hat{b}_{\boldsymbol{k}})$ can be decomposed into three orthogonal components with amplitudes $(B_{\boldsymbol{k}}^{(+)}, B_{\boldsymbol{k}}^{(-)}, B_{\boldsymbol{k}}^{(0)})$ satisfying

$$\frac{\partial B_{\boldsymbol{k}}^{(j)}}{\partial t} + \mathrm{i}\lambda_{\boldsymbol{k}}^{(j)} B_{\boldsymbol{k}}^{(j)} = \sum_{\boldsymbol{k}=\boldsymbol{p}+\boldsymbol{q}} \sum_{r,s=\pm,0} \Gamma_{\boldsymbol{k}\boldsymbol{p}\boldsymbol{q}}^{jrs} B_{\boldsymbol{p}}^{r} B_{\boldsymbol{q}}^{s}. \tag{2.5}$$

In (2.5), j is 0 or $\pm$, where $j = \pm$ correspond to two internal wave modes with frequencies $\lambda_{\boldsymbol{k}}^{(\pm)} = \pm\sigma_k$, while $j = 0$ corresponds to a vortical mode with $\lambda_{\boldsymbol{k}}^{(0)} = 0$. The Γ are the interaction coefficients. Velocity and temperature disturbances with $k_h = 0$ have zero frequency and no PV, so the wave/vortical mode decomposition does not apply to them. The total energy is therefore composed of vortical, wave and $k_h = 0$

https://doi.org/10.1017/S0022112004000977 Published online by Cambridge University Press

contributions, i.e. $E = E^{(0)} + E^{(\pm)} + E^{(S)}$ where

$$E^{(0)} = \frac{1}{2} \sum_{k_h \neq 0} \left| B_{\boldsymbol{k}}^{(0)} \right|^2, \tag{2.6a}$$

$$E^{(\pm)} = \frac{1}{2} \sum_{k_h \neq 0} \left| B_{\boldsymbol{k}}^{(+)} \right|^2 + \left| B_{\boldsymbol{k}}^{(-)} \right|^2, \tag{2.6b}$$

$$E^{(S)} = \frac{1}{2} \sum_{k_h = 0} |\hat{u}_{\boldsymbol{k}}|^2 + |\hat{v}_{\boldsymbol{k}}|^2 + |\hat{b}_{\boldsymbol{k}}|^2 / N^2. \tag{2.6c}$$

We denote the $k_h = 0$ energy with an 'S' for shear, keeping in mind that horizontally averaged temperature as well as velocity are included (unlike Smith & Waleffe 2002).

Nonlinear interactions can be classified according to the number of vortical and wave modes in a wavevector triad. The various classes of interactions are discussed in detail by Lelong & Riley (1991), Godeferd & Cambon (1994), Bartello (1995), Babin *et al.* (1997) and Embid & Majda (1998). For now we simply recall that the approximate triad-wise conservation of Π^2 implies that only $(\pm, 0, 0)$ interactions (i.e. those involving one wave mode and two vortical modes) can exchange energy between vortical and wave motion. In the strongly stratified limit, nonlinear interactions are dominated by resonant interactions satisfying

$$\boldsymbol{k} = \boldsymbol{p} + \boldsymbol{q}, \quad \lambda_k = \lambda_p + \lambda_q. \tag{2.7a,b}$$

The $(\pm, 0, 0)$ interactions are never resonant, yet for small wave frequencies, near-resonant exchanges are possible. The $(\pm, \pm, 0)$ interactions, by contrast, are easy to resonate. Conservation of Π^2 requires that the single vortical mode act as a catalyst, remaining unchanged as energy moves between the two wave modes.

The linear normal mode decomposition reduces to the PV decomposition when the PV is approximately linear in $\boldsymbol{u}$ and b, i.e. when $\Pi \approx \Pi_1$ where

$$\Pi = \Pi_1 + \Pi_2, \tag{2.8}$$

and

$$\Pi_1 = N^2 \omega_z, \quad \Pi_2 = \boldsymbol{\omega} \cdot \nabla b'. \tag{2.9a,b}$$

For vortical motion, scale analysis suggests that this approximation is reasonable when $Fr_z \ll 1$. Π_2 can be shown to scale as $\max(W B_0 / L_h^2, U B_0 / L_h L_z)$ where $w \sim W$ and $b \sim B_0$. Using the fact that (2.1b) implies $W \lesssim U L_z / L_h$, along with the assumption (reasonable for stratified turbulence) that $L_z / L_h \lesssim 1$, one can show that $\Pi_2 \lesssim U B_0 / L H$. Following Riley *et al.* (1981), we scale Π_1 by $N^2 U / L_h$ and B_0 by U^2 / L_z. The ratio of Π_2 to Π_1 is then

$$\frac{\Pi_2}{\Pi_1} \sim Fr_z^2, \tag{2.10}$$

and so Π_1 is a good approximation to Π when $Fr_z \ll 1$. The results of Billant & Chomaz (2001) suggest that this condition is never met, as Fr_z is always $O(1)$. We anticipate, however, that Π_1 will approximate Π at scales larger than U/N; at smaller scales, the linear normal modes have no physical interpretation in terms of either time scales or PV.

https://doi.org/10.1017/S0022112004000977 Published online by Cambridge University Press

3. Inviscid unforced truncated dynamics

Inviscid unforced truncated stratified turbulence can be studied as a problem of equilibrium statistical mechanics. This approach, though limited (real turbulence is far from equilibrium) has proven useful in the past, for example by accounting for the forward energy cascade in three-dimensional turbulence and the inverse energy cascade in two-dimensional turbulence (for a review see Holloway 1986). The Boussinesq equations (2.1) with $\boldsymbol{F}=0$ and $D_u=D_b=0$, truncated cylindrically to a finite number of Fourier modes with k_h, $|k_z|\leqslant k_T$, have one exact invariant: the total energy E. Equilibrium statistical mechanics predicts a macrocanonical probability density function (p.d.f.) of the form

$$P = C\exp(-\alpha E), \tag{3.1}$$

where α and C are constants depending on E. Ensemble-averaged modal energy spectra computed with (3.1) are

$$\left\langle \left|B_{\boldsymbol{k}}^{(j)}\right|^2\right\rangle = 1/\alpha, \tag{3.2}$$

where j is 0 or $\pm$ and $\langle\cdot\rangle$ denotes an ensemble average. Energy is equipartioned among the modes, a well-known result for three-dimensional turbulence (Lee 1952). Equipartition implies that $\langle E^{(\pm)}\rangle = 2\langle E^{(0)}\rangle$ and $\langle E_K\rangle = 2\langle E_P\rangle$, where E_K and E_P are the kinetic and potential energy

$$E_K = \frac{1}{2}\sum_{\boldsymbol{k}} |\hat{u}_{\boldsymbol{k}}|^2 + |\hat{v}_{\boldsymbol{k}}|^2 + |\hat{w}_{\boldsymbol{k}}|^2, \quad E_P = \frac{1}{2}\sum_{\boldsymbol{k}} |\hat{b}_{\boldsymbol{k}}|^2/N^2. \tag{3.3a,b}$$

The untruncated Boussinesq equations are further constrained by the Lagrangian conservation of PV, which generates an infinite number of invariants $[G(\Pi)]$ where G is an analytic function and $[\cdot]$ denotes a spatial average. While none of these invariants survive the spectral truncation, there is an approximate invariant as $(\boldsymbol{u}, b)\to 0$ (Warn 1986; Bartello 1995). In this limit,

$$G(\Pi) \sim G(0) + G'(0)\Pi + \tfrac{1}{2}G''(0)\Pi^2 + O(\Pi^3), \tag{3.4}$$

which upon averaging and retaining only terms up to quadratic order in $(\boldsymbol{u}, b)$ reduces to

$$[G(\Pi)] \sim G(0) + \tfrac{1}{2}G''(0)\left[\Pi_1^2\right] \tag{3.5}$$

(since $[\Pi_1]=0$) where Π_1 is given in (2.9*a*). Since $G(0)$ is constant, there is a second quadratic invariant in the limit of 'weak' flow given by

$$V = \tfrac{1}{2}\left[\Pi_1^2\right] = \tfrac{1}{2}\sum_{\boldsymbol{k}} N^2 k_h^2 \left|B_{\boldsymbol{k}}^{(0)}\right|^2. \tag{3.6}$$

V is proportional to the quadratic part of the potential enstrophy $[\Pi^2/\rho_o^2]$, which as we have seen approximates the full potential enstrophy (invariant when $k_T\to\infty$) well when $Fr_z \ll 1$. Nevertheless, we expect the finite truncation to ultimately destroy the conservation of V.

Assuming that V is exactly conserved, the macrocanonical p.d.f. becomes

$$P = C\exp(-\alpha E - \beta V) \tag{3.7}$$

$$= C\exp\left(-\tfrac{1}{2}\sum_{\boldsymbol{k}} \alpha\left(\left|B_{\boldsymbol{k}}^{(+)}\right|^2 + \left|B_{\boldsymbol{k}}^{(-)}\right|^2\right) + \left(\alpha + \beta k_h^2 N^2\right)\left|B_{\boldsymbol{k}}^{(0)}\right|^2\right), \tag{3.8}$$

https://doi.org/10.1017/S0022112004000977 Published online by Cambridge University Press

yielding modal spectra of vortical and wave energy of the form

$$\left\langle \left|B_{\boldsymbol{k}}^{(0)}\right|^2 \right\rangle = \frac{1}{\lambda_1 + \lambda_2 k_h^2}, \quad \left\langle \left|B_{\boldsymbol{k}}^{(+)}\right|^2 + \left|B_{\boldsymbol{k}}^{(-)}\right|^2 \right\rangle = \frac{2}{\lambda_1}. \tag{3.9a,b}$$

The coefficients $\lambda_1 = \alpha$ and $\lambda_2 = \beta N^2$ depend on E and V. Consider the horizontal and vertical wavenumber spectra of vortical and wave energy, defined as

$$E_h^{(j)}(k_{h_i}) = \frac{1}{2} \sum_{\boldsymbol{k}' \in I_h(k_{h_i})} \left|B_{\boldsymbol{k}'}^{(j)}\right|^2, \quad E_z^{(j)}(k_{z_i}) = \frac{1}{2} \sum_{\boldsymbol{k}' \in I_z(k_{z_i})} \left|B_{\boldsymbol{k}'}^{(j)}\right|^2, \tag{3.10a,b}$$

where j is 0 or $\pm$,

$$I_h(k_{h_i}) = \{\boldsymbol{k}' \,|\, k_{h_i} - \delta/2 \leqslant k_h' < k_{h_i} + \delta/2\}, \tag{3.11a}$$

$$I_z(k_{z_i}) = \{\boldsymbol{k}' \,|\, k_{z_i} - \delta/2 \leqslant |k_z'| < k_{z_i} + \delta/2,\ k_h \neq 0\}, \tag{3.11b}$$

and $\delta = 2\pi/L$. For $L \to \infty$, the modal spectra (3.9) yield horizontal spectra

$$\left\langle E_h^{(0)}(k_h) \right\rangle = \frac{2\pi k_T k_h}{\lambda_1 + \lambda_2 k_h^2}, \quad \left\langle E_h^{(\pm)}(k_h) \right\rangle = \frac{4\pi k_T k_h}{\lambda_1}. \tag{3.12a,b}$$

The vertical wavenumber spectra $E_z^{(0)}(k_z)$ and $E_z^{(\pm)}(k_z)$ are independent of k_z. The vortical energy spectrum $E_h^{(0)}(k_h)$ has a maximum at

$$k_p = \left(\frac{\lambda_1}{\lambda_2}\right)^{1/2}, \tag{3.13}$$

provided that $\lambda_2 > 0$ (see below). These spectra point to an inhibited transfer of vortical energy to large k_h and an efficient transfer to large k_z. Wave energy, on the other hand, is transferred efficiently to small vertical and horizontal scales. In all of the above, we have neglected the contribution of the $k_h = 0$ modes. It is straightforward to show that $E^{(S)}$ is equipartioned along the k_z-axis.

Kraichnan (1967, 1975) used equilibrium statistical mechanics to derive the existence of an inverse energy cascade in two-dimensional turbulence. Given the close resemblance of V to the enstrophy in two dimensions, it is worthwhile to reconsider his argument and apply it to stratified turbulence (see Warn 1986, for the shallow-water equations). Let k_i characterize the initial conditions, defining k_i^2 to be the ratio of enstrophy to energy. The two-dimensional equilibrium energy spectrum has the same form as (3.12a), and when $k_i \ll k_T$ the peak in the spectrum occurs at

$$k_p \sim k_T \exp\left(-k_T^2/2k_i^2\right). \tag{3.14}$$

Therefore, $k_p \to 0$ as $k_T \to \infty$, suggesting an inverse cascade of energy in two-dimensional turbulence.

Stratified turbulence is very different. Integrating (3.9) over all $\boldsymbol{k}$, E and V take the form

$$E = E^{(0)} + E^{(\pm)} = \frac{\pi k_T}{\lambda_2} \log\left(1 + \frac{\lambda_2}{\lambda_1} k_T^2\right) + \frac{2\pi k_T^3}{\lambda_1}, \tag{3.15a}$$

$$V = \frac{N^2 \pi k_T}{\lambda_2} \left(k_T^2 - \frac{\lambda_1}{\lambda_2} \log\left(1 + \frac{\lambda_2}{\lambda_1} k_T^2\right)\right). \tag{3.15b}$$

https://doi.org/10.1017/S0022112004000977 Published online by Cambridge University Press

As in two dimensions, we use the invariants to define a characteristic wavenumber, letting

$$k_i = \left(\frac{V}{N^2 E}\right)^{1/2}. \tag{3.16}$$

Dividing (3.15*b*) by (3.15*a*) and defining $X = \lambda_2 k_i^2/\lambda_1$, we have

$$\frac{k_i^2}{k_T^2}(1+X)\log\left(1+\frac{k_T^2}{k_i^2}X\right) = X(1-2X). \tag{3.17}$$

When $k_i \ll k_T$, the non-trivial solution to (3.17) is $X \sim 1/2$, yielding $\lambda_1 \sim 2\lambda_2 k_i^2$. In this limit, we can simplify (3.15) and show that

$$\lambda_1 \sim \frac{2\pi k_T^3}{E}, \quad \lambda_2 \sim \frac{\pi N^2 k_T^3}{V}, \tag{3.18a,b}$$

implying that the maximum vortical energy occurs at $k_p \sim \sqrt{2}k_i$. The spectrum is peaked at a finite k_h as $k_T \to \infty$, a conclusion which is analogous to Warn's (1986) result for shallow water. Rather than cascading upscale, vortical energy is transferred to forward-cascading wave energy in significant quantities. The spectral peak in k_h remains unchanged.

These predictions for the inviscid unforced truncated dynamics can be tested by integrating (2.1) with $\boldsymbol{F} = 0$ and $D_u = D_b = 0$. We have performed a computation with a pseudo-spectral code at a low resolution of 32^3, with $L = 2\pi$ and $N = 8$. Leapfrog time stepping was employed along with a Robert filter with parameter 0.0005 to control the computational mode (Asselin 1972). Aliasing errors were eliminated by truncating cylindrically at $k_T = 10$. Initial energy was peaked around $k_h = 3$ and $k_z = 0$, and was 90% vortical. Froude numbers, computed as

$$Fr_h = \frac{\sqrt{[\omega_z^2]}}{N}, \quad Fr_z = \frac{\sqrt{[\omega_x^2+\omega_y^2]/2}}{N}, \tag{3.19a,b}$$

had initial values of $Fr_h = 0.1$ and $Fr_z = 0.05$.

V varies by approximately 100% over the course of the simulation, and the equilibrium (3.9) is not attained (smaller Froude numbers yield similar results when time is rescaled). Instead, the system evolves to the energy equipartition spectrum (3.2), as shown in figure 1. Nevertheless, an intermediate equilibrium appears to be reached, based on the approximate conservation of $E^{(0)}$, $E^{(\pm)}$ and V. We compute the 'decoupled' equilibrium assuming these three invariants, yielding the spectra

$$\left\langle \left|B_{\boldsymbol{k}}^{(0)}\right|^2 \right\rangle = \frac{1}{\lambda_3 + \lambda_2 k_h^2}, \quad \left\langle \left|B_{\boldsymbol{k}}^{(+)}\right|^2 + \left|B_{\boldsymbol{k}}^{(-)}\right|^2 \right\rangle = 2/\lambda_1, \tag{3.20a,b}$$

where λ_1 depends on $E^{(\pm)}$, while λ_2 and λ_3 depend on $E^{(0)}$ and V (see Bartello 1995, for the rotating stratified case). If the system relaxes to (3.20) on a shorter time scale than that of the variations in $E^{(0)}$, $E^{(\pm)}$ and V, we should find spectra which are close to (3.20) defined by instantaneous values of the 'invariants'. Indeed, this is exactly what we observe. In figure 2 we plot the computed k_h spectra along with the instantaneous decoupled equilibrium at three different times; the agreement in each case is quite good. The $k_h = 0$ modes were excluded from the computation because the time scale of their growth is much larger than the other time scales of the problem. Because the turbulence seems to relax to this 'instantaneous equilibrium' over a relatively short time scale, it would appear to have relevance to the non-equilibrium forced-dissipative

https://doi.org/10.1017/S0022112004000977 Published online by Cambridge University Press

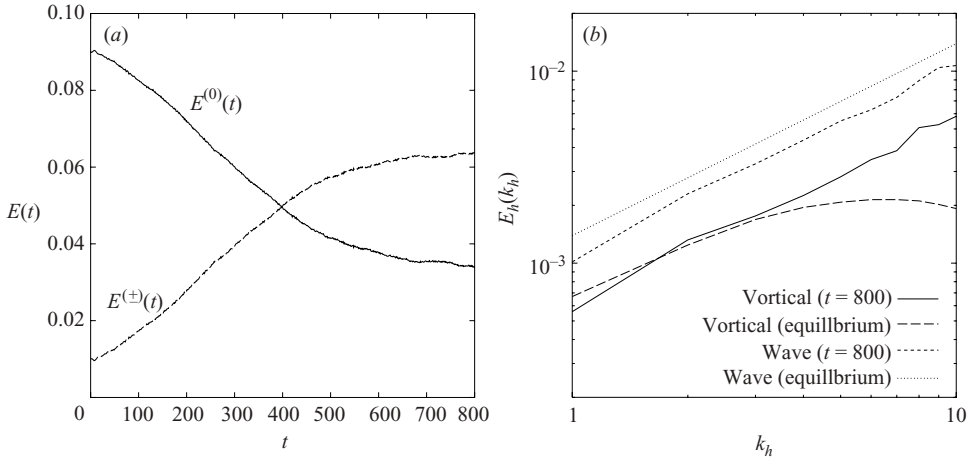


FIGURE 1. (*a*) Time series of vortical and wave energy over the course of the inviscid simulation, and (*b*) the horizontal wavenumber spectra of vortical and wave energy at $t = 800$, along with the statistical equilibrium spectra (3.12).

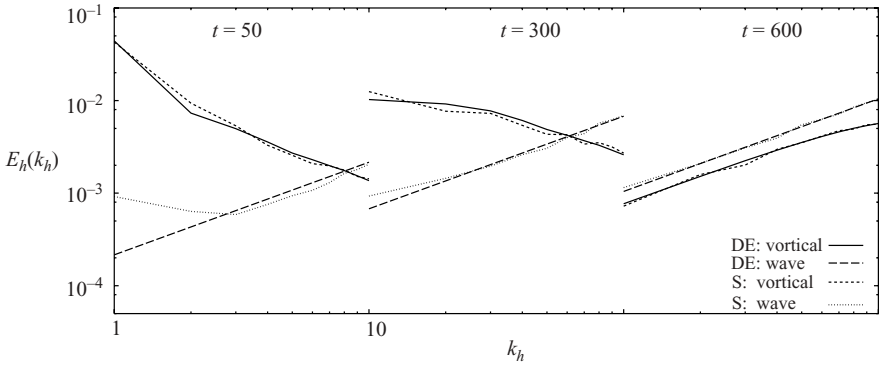


FIGURE 2. The horizontal wavenumber spectra of vortical and wave energy of the decoupled equilibrium (3.20) ('DE') and simulation ('S') at $t = 50$ (left), $t = 300$ (middle) and $t = 600$ (right).

problem. The inviscid analysis suggests that large-scale vortical motion leaks energy into forward-cascading internal waves, while the remaining vortical motion preserves its horizontal scale and develops small scales in the vertical.

4. Forced–dissipative simulations

4.1. *Numerical approach*

Keeping in mind the nature of the inviscid dynamics, we now consider stratified turbulence with forcing and dissipation. The Boussinesq equations (2.1) were integrated on a cubic domain with $L = 2\pi$. Rather than using a small-aspect-ratio domain like Laval *et al.* (2003), we have chosen to let the flow determine the aspect ratio. As in the inviscid simulation, the pseudo-spectral method was employed along with the leapfrog time-stepping scheme and a Robert filter parameter of 0.004. Because of the long integration times required to reach statistical stationarity, simulations

https://doi.org/10.1017/S0022112004000977 Published online by Cambridge University Press

were spun up at a modest resolution of 90^3 and then continued at 180^3. The resolution was increased once all the 90^3 runs had reached stationarity. Aliasing errors were eliminated by truncating cylindrically, with $k_T = 29$ at 90^3 and 59 at 180^3. Cylindrical hyperviscosity and hyperdiffusion were used for the dissipation operators:

$$D_u = \nu_h(-1)^{n+1}\nabla_h^{2n} + \nu_z(-1)^{n+1}\left(\frac{\partial}{\partial z}\right)^{2n}, \tag{4.1a}$$

$$D_b = \kappa_h(-1)^{n+1}\nabla_h^{2n} + \kappa_z(-1)^{n+1}\left(\frac{\partial}{\partial z}\right)^{2n}. \tag{4.1b}$$

We take $\nu_h = \nu_z = \kappa_h = \kappa_z \equiv \nu$. A value of $n > 1$ artificially compresses the dissipation range, allowing for a longer inertial range. We use $n = 4$, as in Bartello, Métais & Lesieur (1996). Hyperviscosity modifies the definition of the dissipation wavenumber, which becomes

$$k_d = \left(\frac{\epsilon}{\nu^3}\right)^{1/(6n-2)}. \tag{4.2}$$

Forcing was employed in order to attain statistical stationarity, which allows the straightforward analysis of the dependence of various quantities on Froude numbers. The velocity forcing function $\boldsymbol{F}$ was restricted to vertically uniform vortical motion, with

$$\hat{F}_j(\boldsymbol{k}, t) = \begin{cases} A(k_h)G_j(\boldsymbol{k}, t), & k_z = 0 \\ 0, & k_z \neq 0, \end{cases} \tag{4.3}$$

where j is x or y and $\hat{F}_z = 0$. $G_x(\boldsymbol{k}, t)$ and $G_y(\boldsymbol{k}, t)$ are Gaussian random processes with zero mean satisfying $k_x G_x + k_y G_y = 0$. The forcing amplitude $A(k_h)$ is a quadratic function of k_h centred at the forcing wavenumber k_f, given by

$$A(k_h) = \begin{cases} a(k_f + 1 - k_h)(k_h - k_f + 1), & k_f - 1 \leqslant k_h \leqslant k_f + 1 \\ 0, & |k_h - k_f| > 1. \end{cases} \tag{4.4}$$

A small amount of random seed energy ensured that vertical structure would emerge spontaneously. $G_x(\boldsymbol{k}, t)$ and $G_y(\boldsymbol{k}, t)$ are uncorrelated in $\boldsymbol{k}$ and have a decorrelation time scale of around $25\Delta t$. Our forcing follows that of Herring & Métais (1989), although the horizontal length scales differ. Herring & Métais (1989) forced at small horizontal scales to allow for a possible inverse cascade of energy. We have chosen to force at large scales ($k_f = 3$) to maximize the spectral range between k_f and k_d, since our interest is in the three-dimensionalization of large-scale geophysical vortices.

A set of ten simulations was performed, covering the range of Brunt–Väisälä frequencies $1/4 \leqslant N \leqslant 32$ corresponding to $10^{-2} < Fr_h < 10$. We chose this range so that the lowest stratification would have $Fr_h > 1$ and the strongest stratification would suppress all overturning. Identical values of a, Δt and ν were used for each N, with $a = 0.09$, $\Delta t = 0.004$, and $\nu = 1.90 \times 10^{-11}$ at low resolution and 1.18×10^{-13} at high resolution. The Kolmogorov wavenumber k_d is approximately 43 at high resolution.

4.2. *Simulation of the reduced equations*

Before presenting these numerical simulations, it is worth examining the limiting behaviour of vortical mode dynamics. We follow Embid & Majda (1998) who, having averaged the Boussinesq equations over the wave time scale to remove the wave part

https://doi.org/10.1017/S0022112004000977 Published online by Cambridge University Press

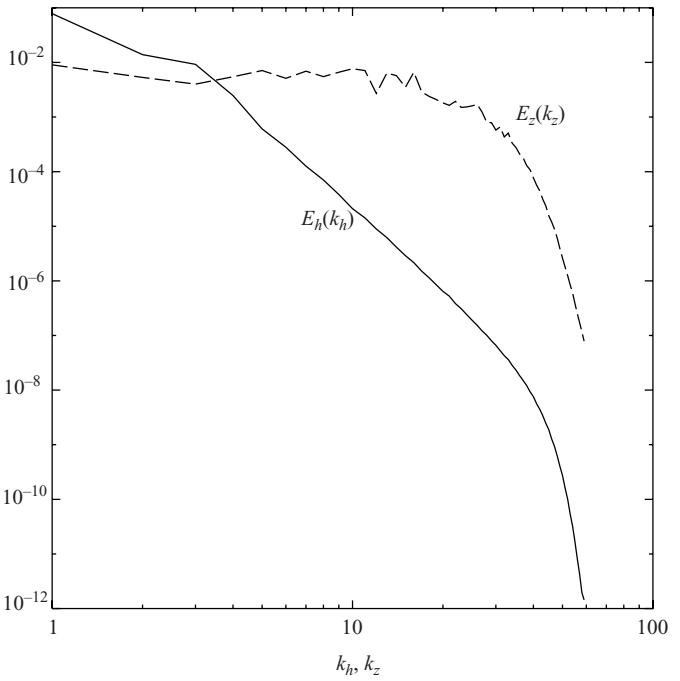


FIGURE 3. Time-averaged horizontal and vertical wavenumber energy spectra from a simulation of the reduced equations (4.6) subjected to the forcing and dissipation described in §4.1. The spectra were averaged at statistical stationarity over several nonlinear turnover times.

of $\boldsymbol{u}$ and b, decomposed the horizontal velocity into a horizontally uniform ($k_h = 0$) and vortical component

$$\boldsymbol{u}_h = \boldsymbol{V}_h(z,t) + \hat{\boldsymbol{z}} \times \nabla_h \psi, \tag{4.5}$$

where ψ is the stream function for the vortical motion. The reduced equations for vortical motion, valid for Fr_h, $Fr_z \to 0$, are (neglecting forcing and dissipation)

$$\frac{\partial \zeta}{\partial t} + \boldsymbol{u}_h \cdot \nabla_h \zeta = 0, \tag{4.6a}$$

$$\frac{\partial b'}{\partial t} = 0, \tag{4.6b}$$

$$\frac{\partial \boldsymbol{V}_h}{\partial t} = 0, \tag{4.6c}$$

where $\zeta = \nabla_h^2 \psi$ is the vertical vorticity and $w = 0$. The limiting dynamics consist of decoupled layers of horizontal flow which satisfy the equations for two-dimensional turbulence at every level. The velocity $\boldsymbol{V}_h(z,t)$ decouples from the rest of the flow, implying that the growth rate of $E^{(S)}$ should go to zero as Fr_h, $Fr_z \to 0$.

We have performed a simulation of the reduced system (4.6) with $\boldsymbol{V}_h = 0$, following the approach described in §4.1. The resulting vertical spectrum of energy is approximately flat, while the horizontal spectrum is steep (with a slope near -5) out to the dissipation range (figure 3). The emergence of a flat vertical spectrum follows immediately from the interpretation of the limiting dynamics as decoupled layers of horizontal flow. By 'decoupled', we mean that the velocity correlation at two points

https://doi.org/10.1017/S0022112004000977 Published online by Cambridge University Press

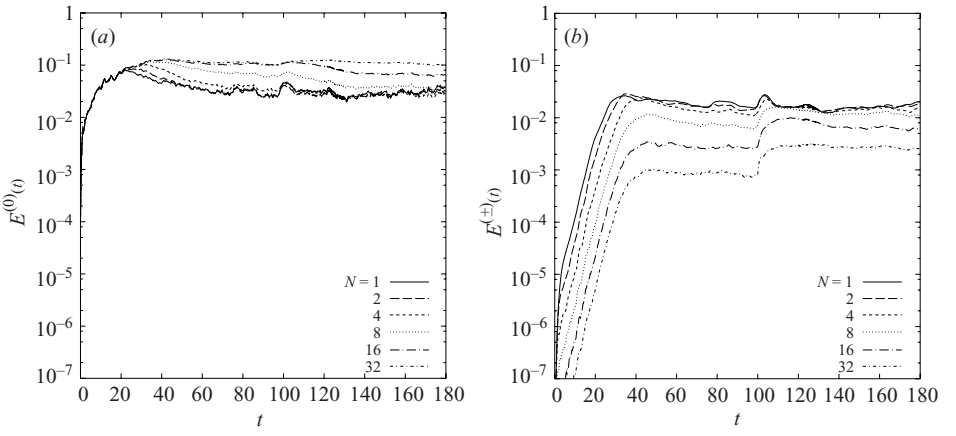


FIGURE 4. Time series of (*a*) vortical energy $E^{(0)}(t)$ and (*b*) wave energy $E^{(\pm)}(t)$ for $N = 1$, 2, 4, 8, 16 and 32.

goes rapidly to zero as the vertical separation between the points increases. Assume that

$$\langle u_i(\boldsymbol{x}, t)u_i(\boldsymbol{x} + \boldsymbol{r}, t)\rangle = C(\boldsymbol{r}_h, t)\exp(-|r_3|/l), \tag{4.7}$$

where $\boldsymbol{r} = (r_1, r_2, r_3)$ is the separation between the two points, $\boldsymbol{r}_h = (r_1, r_2)$, l is the correlation length, $\langle\cdot\rangle$ denotes an ensemble average (in practice, a time average), and statistical homogeneity is assumed. The modal kinetic energy spectrum is defined as the Fourier transform of (4.7) (e.g. Lesieur 1997), which reduces to

$$U(\boldsymbol{k}, t) = \frac{1}{(2\pi)^3}\frac{2l}{1 + (lk_z)^2}\int\int C(\boldsymbol{r}_h, t)\exp(-\mathrm{i}\boldsymbol{k}_h \cdot \boldsymbol{r}_h)\,\mathrm{d}\boldsymbol{r}_h \tag{4.8}$$

as $L \to \infty$. $U(\boldsymbol{k}, t)$ is approximately independent of k_z when $k_z \ll 1/l$. The vertical wavenumber spectrum (obtained by integrating $U(\boldsymbol{k})$ over $\boldsymbol{k}_h$) is therefore independent of k_z at scales larger than the correlation length, a direct result of the vertical decoupling.

4.3. *Simulations of the full equations*

Returning to the full Boussinesq equations, time series of vortical and wave energy are shown in figure 4. The vortical energy grows rapidly at first and, until around $t = 20$, the simulations evolve nearly identically. The forced flow during this interval is approximately two-dimensional, so there is minimal energy dissipation. Vertical gradients eventually emerge and dissipation balances the forcing on a time scale which increases with N. The initial exponential growth rate of wave energy appears to be independent of N, which was also noted by Herring & Métais (1989). A jump in the wave energy is visible at $t = 100$, when the resolution was increased from 90^3 to 180^3. This jump suggests that a significant amount of wave energy is present at small scales.

The simulations were run to $t = 180$, and a number of quantities were output over the stationary range of $130 \leqslant t \leqslant 180$ at an interval of $\Delta t_{out} = 0.25$. All statistics were averaged over this interval. The vortical energy spectrum was used to define vertical and horizontal turnover times as

$$\tau_z = \frac{2\pi}{\overline{k_z}U}, \quad \tau_h = \frac{2\pi}{\overline{k_h}U}, \tag{4.9a,b}$$

https://doi.org/10.1017/S0022112004000977 Published online by Cambridge University Press

N	τ_z	τ_h	Fr_z	Fr_h	k_b	N	τ_z	τ_h	Fr_z	Fr_h	k_b
1/4	19	6.4	6.2	5.8	3.5	3	4.5	8.3	0.65	0.33	150
1/2	15	6.5	3.0	2.7	11	4	3.4	8.8	0.55	0.21	220
1	11	7.1	1.5	1.3	31	8	2.1	10	0.34	0.072	590
3/2	8.4	7.4	1.1	0.79	55	16	1.5	10	0.20	0.034	1600
2	6.8	7.6	0.85	0.57	83	32	1.2	9.8	0.12	0.018	4200

TABLE 1. Nonlinear turnover times, Froude numbers and buoyancy wavenumbers for all of the runs, based on time averages over $130 \leqslant t \leqslant 180$.

where

$$\overline{k}_z = \left(\frac{\int k_z^{1/2} E_z^{(0)}(k_z)\,\mathrm{d}k_z}{\int E_z^{(0)}(k_z)\,\mathrm{d}k_z} \right)^2, \quad \overline{k}_h = \left(\frac{\int k_h^{1/2} E_h^{(0)}(k_h)\,\mathrm{d}k_h}{\int E_h^{(0)}(k_h)\,\mathrm{d}k_h} \right)^2, \tag{4.10a,b}$$

$$U = \left(2\,E^{(0)}\right)^{1/2}, \tag{4.11}$$

and $E^{(0)}$ is the time-averaged vortical energy. The definition of $\overline{k}_z$ and $\overline{k}_h$ is non-standard, and will be explained in greater detail below. The length of the averaging interval $130 \leqslant t \leqslant 180$ expressed in terms of τ_h and τ_z depends on N, and varies from $3\tau_z$ to $41\tau_z$ and $5\tau_h$ to $8\tau_h$. Table 1 gives τ values for each of the runs. Froude numbers as defined in (3.19) are also given; Fr_z varies between 0.12 and 6.2, while Fr_h varies between 0.018 and 5.8. Despite the prediction of Billant & Chomaz (2001) (supported by the simulations of Godeferd & Staquet 2003) that $Fr_z \sim O(1)$ for all N, we find that Fr_z decreases monotonically with N, although it does so less rapidly than Fr_h. The horizontal and vertical Froude numbers vary differently with N because L_z, unlike L_h, collapses as N increases. Below we will see that when U and L_z are measured separately, rather than together in the r.m.s. horizontal vorticity, our simulations are more consistent with the Billant & Chomaz (2001) scaling, at least at moderate stratifications. At finite Reynolds number Re, L_z is bounded below by the Kolmogorov length scale; in this case, both Fr_h and $Fr_z \to 0$ as $N \to \infty$. The effect of finite Re is not accounted for by Billant & Chomaz (2001). The Reynolds number in our simulations, defined as $Re = (k_d/\overline{k}_h)^{4/3}$, varies between 30 (for $N = 1/4$) and 100 (for $N = 32$).

Snapshots of vorticity for $N = 1$, 4 and 16 are shown in figure 5. When $N = 1$, Fr_h and $Fr_z \sim O(1)$ and the turbulence appears to be approximately isotropic. When $N = 4$, the effects of the stratification are visible: we see strong layering in the vertical plane, with overturning at small scales. In the horizontal plane, large-scale vortical motion is evident, although small-scale eddies associated with overturning are also present. When $N = 16$, no overturning is visible, and the horizontal profile of ω_z resembles two-dimensional turbulence. In fact, no overturning occurs at any time during the $N = 16$ simulation, which can be seen by examining the p.d.f. of local Richardson number

$$Ri(\boldsymbol{x}, t) = \frac{N^2 + \partial b'/\partial z}{\omega_x^2 + \omega_y^2}, \tag{4.12}$$

in figure 6 (see Métais & Lesieur 1992, for a discussion of the p.d.f. of the related quantity $\partial b'/\partial z$). In all cases, the p.d.f. drops off rapidly for negative values of Ri,

https://doi.org/10.1017/S0022112004000977 Published online by Cambridge University Press

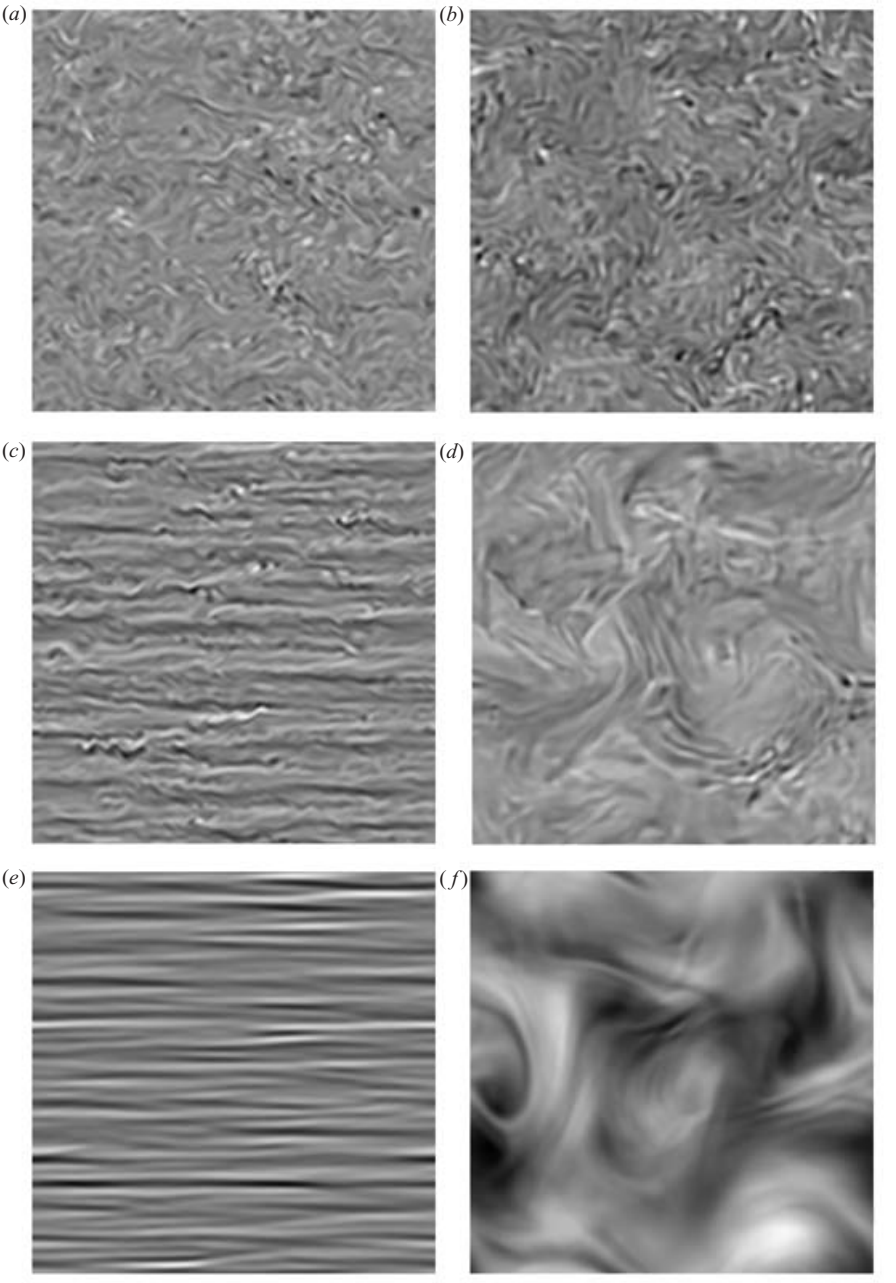


FIGURE 5. Vertical slices (x, z) of ω_y (left column) and horizontal slices (x, y) of ω_z (right column) for (a,b) $N=1$, (c,d) $N=4$ and (e,f) $N=16$ at $t=180$.

which result from overturning density surfaces. As N is increased from 8 to 16, overturning is completely suppressed by stratification and dissipation. This regime is not particularly relevant to atmosphere and ocean dynamics, although it is the limit represented by the reduced equations at finite Re.

https://doi.org/10.1017/S0022112004000977 Published online by Cambridge University Press

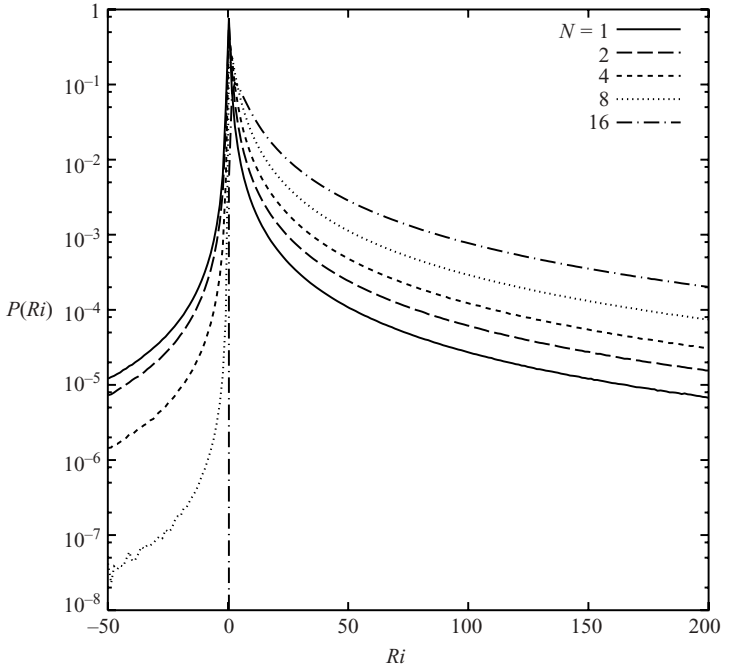


FIGURE 6. The p.d.f. of local Richardson number Ri for $N = 1$, 2, 4, 8 and 16. Only the segment $-50 \leqslant Ri \leqslant 200$ is shown.

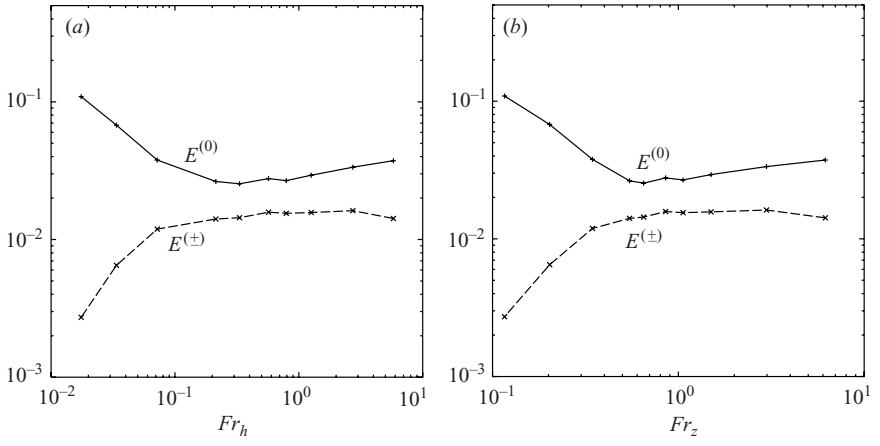


FIGURE 7. Total vortical and wave energy as functions of (*a*) Fr_h and (*b*) Fr_z.

4.3.1. *Integrated quantities*

In figure 7 we plot the time-averaged vortical and wave energies as functions of Fr_h and Fr_z. As the Froude numbers go to zero below $Fr_h = 0.3$, the vortical energy increases while the wave energy drops. At weaker stratifications, the wave energy is approximately independent of Fr_h and Fr_z, while the vortical energy grows marginally as they increase. Presumably, this growth will stop at larger Froude numbers. It is important to recall that at the relatively weak stratifications of Fr_h, $Fr_z \gtrsim 1$, the decomposition of energy into vortical and wave contributions has no real physical

https://doi.org/10.1017/S0022112004000977 Published online by Cambridge University Press

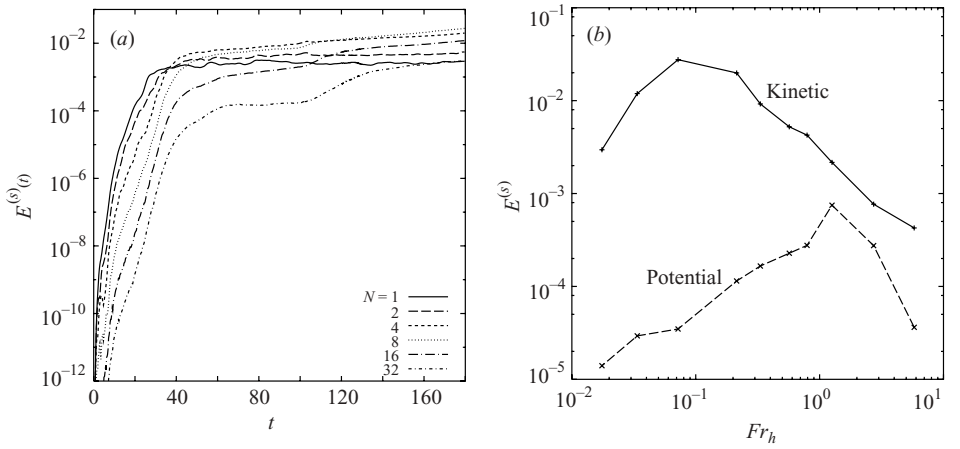


FIGURE 8. (*a*) Time series of $E^{(S)}$ for $N = 1$, 2, 4, 8, 16 and 32, and (*b*) totals of kinetic and potential energy in $E^{(S)}$ plotted against Fr_h at $t = 180$.

significance. Note that the two plots in figure 7 are qualitatively the same; in what follows, we will plot integrated quantities against Fr_h only.

The $k_h = 0$ energy $E^{(S)}$ grows slowly for the duration of our simulations, with a growth rate that depends on N (figure 8*a*). In figure 8(*b*), we plot the kinetic and potential energy of the $k_h = 0$ modes. The potential energy decreases as Fr_h is reduced below 1, where it is at least an order of magnitude smaller than the kinetic energy. The kinetic energy increases as Fr_h decreases down to 0.07, but it drops significantly at stronger stratifications. This drop is not surprising, given that the horizontally averaged horizontal momentum equations,

$$\frac{\partial \overline{u}}{\partial t} = -\frac{\partial}{\partial z}\overline{uw} + D_u\overline{u}, \tag{4.13a}$$

$$\frac{\partial \overline{v}}{\partial t} = -\frac{\partial}{\partial z}\overline{vw} + D_u\overline{v}, \tag{4.13b}$$

imply that vertical velocity is required to transfer energy into the $k_h = 0$ modes. In our simulations, vertical velocity is generated by transfers into internal waves and overturning. The drop in $k_h = 0$ kinetic energy for $Fr_h < 0.07$ is consistent with the suppression of overturning and the corresponding reduction in wave energy. The fact that Smith & Waleffe (2002) did not observe such a drop may be because they forced vertical velocity directly, or it may be that their stratifications were not sufficiently strong. Our results agree with the prediction that the $k_h = 0$ modes decouple from the rest of the flow in the limit of strong stratification (Embid & Majda 1998).

4.3.2. *Energy spectra*

Spectra of wave energy (for a subset of the runs) are shown in figure 9(*a*, *b*). The horizontal spectra (figure 9*a*) steepen as N increases, with spectral slopes varying between -1 and nearly -6. Unlike Laval *et al.* (2003), there are no significant bumps at large k_h in our spectra, probably because of our lower horizontal resolution (necessary for an isotropic computational domain) and more conservative choice of ν. The vertical spectra (figure 9*b*) are peaked at a wavenumber which increases with stratification. For the largest N, this peak occurs near k_d and the spectrum has positive slope out to the dissipation range, as in Laval *et al.* (2003). These results suggest

https://doi.org/10.1017/S0022112004000977 Published online by Cambridge University Press

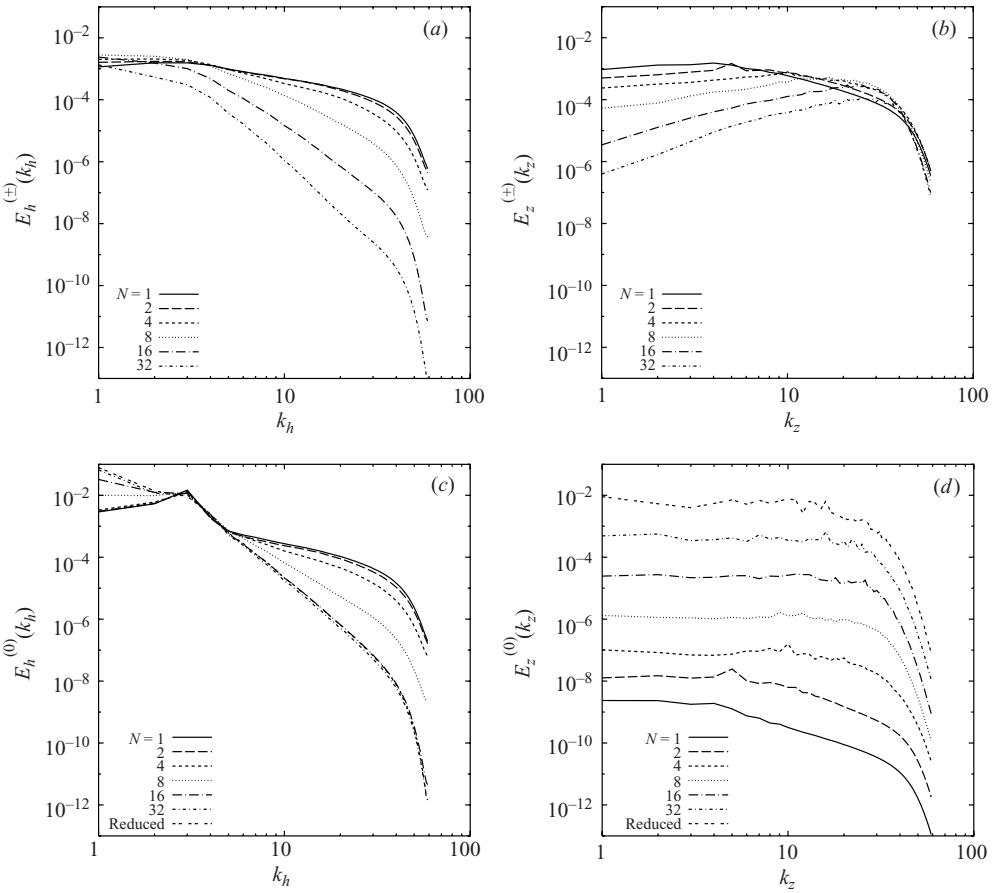


FIGURE 9. Horizontal and vertical wavenumber spectra of wave energy (*a*) $E_h^{(\pm)}(k_h)$, (*b*) $E_z^{(\pm)}(k_z)$, and vortical energy (*c*) $E_h^{(0)}(k_h)$, and (*d*) $E_z^{(0)}(k_z)$ for $N = 1$, 2, 4, 8, 16 and 32 as well as for the reduced equations. Note that in (*d*), the spectra have been offset from one another by factors of 10 for clarity. The reduced equations spectrum is unshifted.

that the nonlinear transfer of vortical energy to wave energy occurs at a decreasing vertical scale as N increases. Because of the existence of overturning in some of our simulations, part of this wave energy may in fact be small-scale turbulence projecting onto the linear wave modes.

The vortical energy spectra are displayed in figure 9(*c*,*d*). For $N \leqslant 2$, the k_h spectra (figure 9*c*) are nearly identical, with slopes slightly shallower than $-5/3$. As N increases beyond 2, the spectra steepen, and appear to saturate at large N with a slope of -5. Indeed, those for $N = 16$ and $N = 32$ are indistinguishable from the spectrum of the reduced equations. Similar spectra were obtained by Laval *et al.* (2003). The vertical spectra (figure 9*d*) are approximately flat at low k_z; these wavenumbers correspond to vertical scales decoupled from one another by the stable stratification. At larger wavenumbers, the decoupling is broken by overturning and dissipation, and the spectra have a non-zero slope. As N increases, the flat range extends to larger k_z while the negative slope range narrows and steepens (see also figure 10, which gives the k_z spectra of vortical energy for all runs with $N \leqslant 4$). For $N = 1$–2, the slope is around -2; at larger N, the range is too narrow to identify a slope. Our results

https://doi.org/10.1017/S0022112004000977 Published online by Cambridge University Press

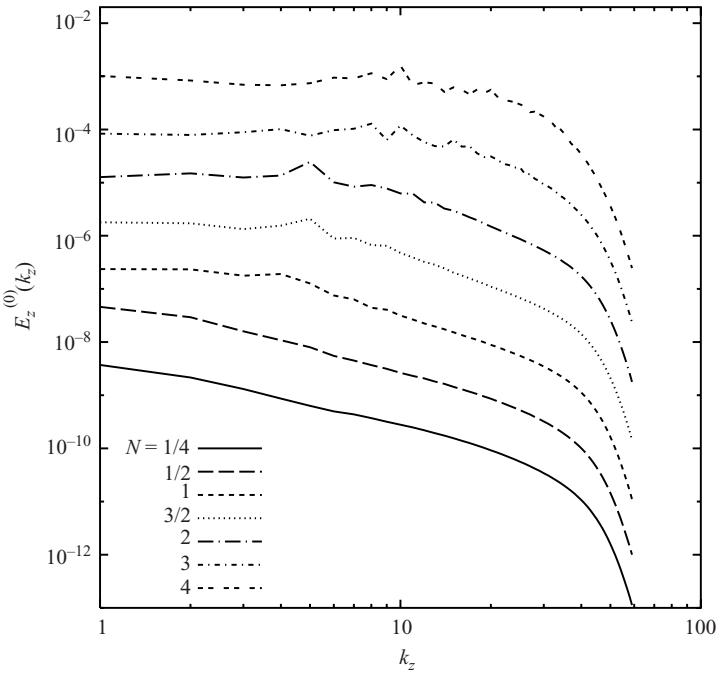


FIGURE 10. Vertical wavenumber spectra of vortical energy $E_z^{(0)}(k_z)$ for $N = 1/4$, 1/2, 1, 3/2, 2, 3 and 4. The spectra have been offset from one another by factors of 10 for clarity. The $N = 4$ spectrum is unshifted.

imply that when overturning is suppressed, the vortical spectra take the form k_h^{-5} and k_z^0, and the dynamics are represented well by the reduced equations. Recall that the equilibrium statistical mechanics also predicts a flat vertical spectrum due to the equipartition of energy in k_z.

The anisotropy of the turbulence can be illustrated by the joint k_h–k_z spectra $E_{hz}^{(0)}(k_h, k_z)$ and $E_{hz}^{(\pm)}(k_h, k_z)$, which are plotted for three different stratifications in figure 11. The lack of dependence of the vortical spectrum on k_z can be seen to extend to larger k_z as N increases. The wave spectrum displays a maximum which, as N increases, moves in towards the k_z-axis and out towards large k_z. This region of the k_h–k_z plane is associated with the low frequencies of the internal wave dispersion relation, and is exactly where we expect the exchange between vortical and wave modes via the $(\pm, 0, 0)$ interaction to be the least off-resonant. At the largest wavenumbers, the spectra are influenced by the cylindrical dissipation operator. However, the anisotropy at small wavenumbers appears to be a robust feature at large N. To verify this point, we have performed an additional simulation at $N = 16$ with spherical truncation and dissipation. The dissipation range is modified by the change in D_u and D_b, but the form of the vortical spectrum at large scales is unchanged (not shown).

4.3.3. *Energy dissipation and transfer*

Consider next the energy dissipation rate, decomposed into contributions from the vertical and horizontal dissipation of vortical and wave energy. One can show that

$$\epsilon_r^{(j)} = 2\nu_r \int_0^{k_T} k_r^{2n} E_r^{(j)}(k_r)\, \mathrm{d}k_r, \tag{4.14}$$

https://doi.org/10.1017/S0022112004000977 Published online by Cambridge University Press

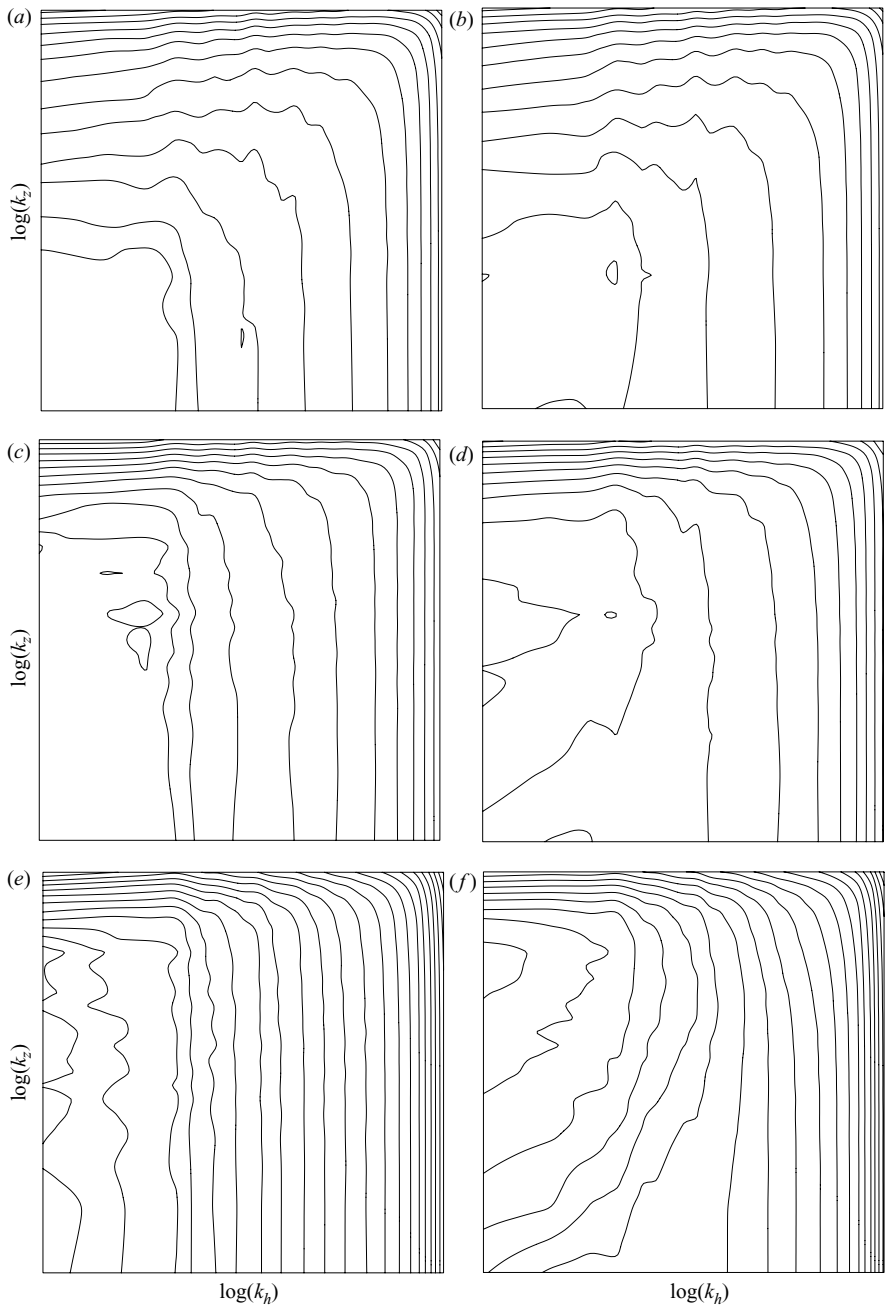


FIGURE 11. Contours of $\log E_{hz}^{(0)}(k_h, k_z)$ (left) and $\log E_{hz}^{(\pm)}(k_h, k_z)$ (right) for (a,b) $N=1$, (c,d) $N=4$ and (e,f) $N=16$. The k_h and k_z coordinates range logarithmically from 1 to 59, and the contour interval in each case is 0.5. Note that since the contours are plotted in the $\log(k_h)$–$\log(k_z)$ plane, isotropic fields appear boxy rather than circular, with box corners at 45° from the axes. Anisotropy is manifested in rectangular boxes, as in (e).

where r is h or z and j is 0 or $\pm$, is the dissipation rate of j-energy in the r-direction. We plot the ϵ against Fr_h in figure 12. When the stratification is weak, the dissipation is nearly isotropic. As the stratification is increased and the horizontal

https://doi.org/10.1017/S0022112004000977 Published online by Cambridge University Press

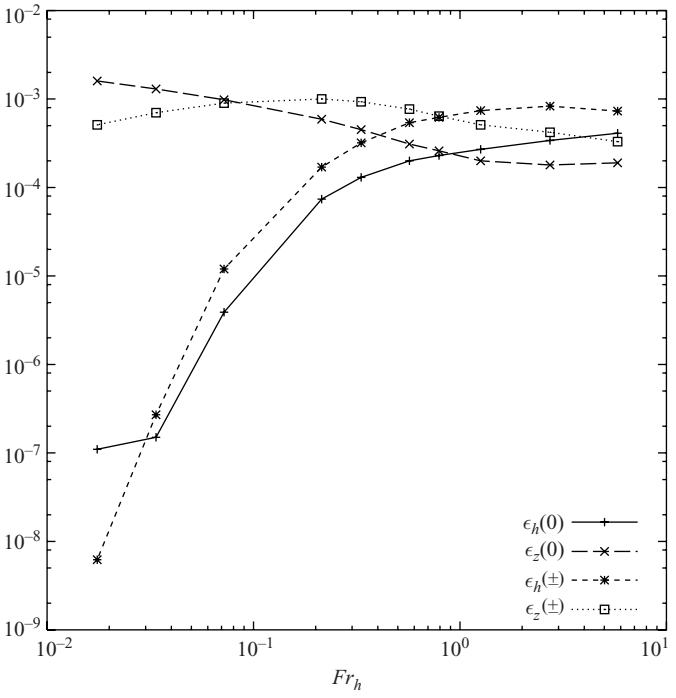


FIGURE 12. Dissipation rates $\epsilon_i^{(j)}$ corresponding to the horizontal and vertical dissipation of vortical and wave energy, as functions of Fr_h.

energy spectra steepen, the horizontal dissipation decreases and is overtaken by the vertical dissipation, as in Fincham *et al.* (1996), when $Fr_h < 0.6$. Overturning and small-scale turbulence, the mechanisms by which structures of small horizontal scale dissipate energy, are suppressed with increasing stratification. In addition, the dissipation of vortical energy exceeds that of wave energy as Fr_h decreases below 0.07. At these strong stratifications, no overturning occurs, and energy is dissipated from the layered vortical motion directly by the vertical derivatives of (4.1).

The vortical and wave spectral energy transfer functions are defined by

$$T^{(j)}(\boldsymbol{k}) = 2\,\mathrm{Re} \sum_{\boldsymbol{k}=\boldsymbol{p}+\boldsymbol{q}} \Gamma^{jrs}_{\boldsymbol{k}\boldsymbol{p}\boldsymbol{q}} B^{(j)^*}_{\boldsymbol{k}} B^{(r)}_{\boldsymbol{p}} B^{(s)}_{\boldsymbol{q}}, \tag{4.15}$$

where j is 0 or $\pm$, $*$ denotes complex conjugate, and the r and s are summed over $\pm$ and 0. Positive $T^{(j)}(\boldsymbol{k})$ denotes a net injection of 'j'-energy into $\boldsymbol{k}$ by nonlinear interactions. To get a clearer picture of the exchange of wave and vortical energy, we decompose the transfer into contributions from the various classes of triads:

$$T^{(j)}(\boldsymbol{k}) = T^{(j,0,0)}(\boldsymbol{k}) + T^{(j,\pm,\pm)}(\boldsymbol{k}) + T^{(j,\pm,0)}(\boldsymbol{k}), \tag{4.16}$$

where j is 0 or $\pm$. For example, $T^{(\pm,0,0)}(\boldsymbol{k})$ represents the transfer of wave energy due to triads of one wave mode and two vortical modes; $T^{(0,\pm,0)}(\boldsymbol{k})$ represents the transfer of vortical energy due to the same class of triads. As we saw above in (2.10) and (3.6), V is increasingly a quadratic invariant (conserved triad-wise) as $Fr_z \to 0$; since only vortical modes contribute to V in this limit, it follows that $(0, \pm, \pm)$ interactions

https://doi.org/10.1017/S0022112004000977 Published online by Cambridge University Press

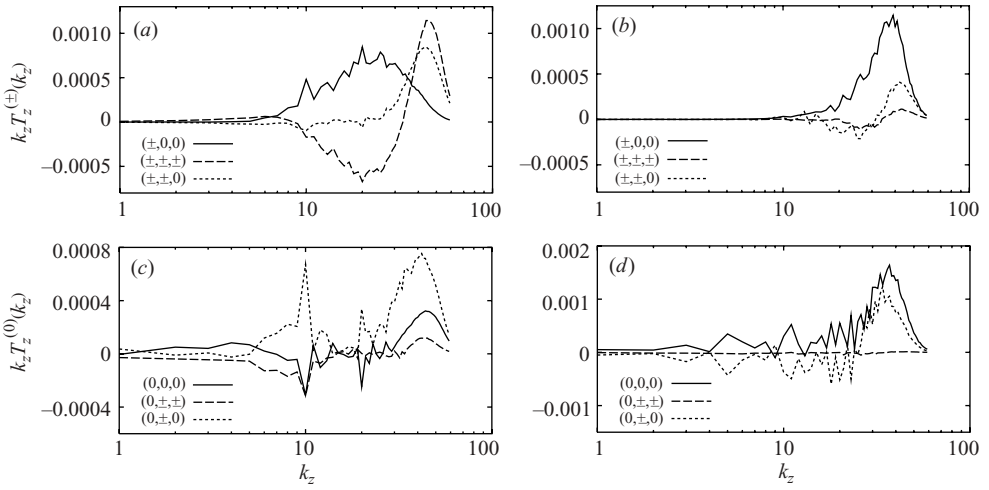


FIGURE 13. The decomposition of the energy transfer spectra $T_z^{(j)}(k_z)$ into contributions from the various classes of triads. The wave (top) and vortical (bottom) transfer spectra are given for $N=4$ (left) and $N=16$ (right). Note that the $(\pm,\pm,\pm)$, $(\pm,\pm,0)$, and $(0,0,0)$ transfers sum to zero independently when the $k_z=0$ contribution (not shown) is accounted for. The transfer is multiplied by k_z so that area is preserved with log-linear coordinates.

cannot modify the vortical mode without violating the conservation of V, and so $T^{(0,\pm,\pm)} \to 0$. Furthermore, off-resonant interactions are suppressed, implying that $T^{(0,\pm,0)}(\boldsymbol{k})$ and $T^{(\pm,0,0)}(\boldsymbol{k}) \to 0$. However, it is the near-resonant triads (of two vortical modes and a low-frequency wave) that exchange energy between vortical and wave modes. In figure 13, we plot the decomposition of the transfer in k_z for $N=4$ and $N=16$. When $N=4$, the injection of vortical energy into the wave energy spectrum $T_z^{(\pm,0,0)}$ has a maximum near $k_z \sim 20$ (figure 13*a*) and $k_h=3$ (not shown), and so the wave modes involved have low frequencies, as expected. The injected wave energy is swept downscale by the three-wave $(\pm,\pm,\pm)$ interaction, and to a lesser extent by the catalytic $(\pm,\pm,0)$ interaction, possibly in the form of wave-breaking and small-scale turbulence. The drain of large-scale vortical energy into wave energy by the $(\pm,0,0)$ interaction represents the 'wave drag' and is a reason why an inverse cascade of vortical energy does not occur in stratified turbulence. When $N=16$ (figure 13*b*), wave energy is injected near k_d. A small amount of wave energy is sent downscale by the $(\pm,\pm,0)$ and $(\pm,\pm,\pm)$ interactions. As Fr_h and $Fr_z \to 0$, interactions collapse onto the resonant set, which is larger for $(\pm,\pm,0)$ triads than for $(\pm,\pm,\pm)$ triads. In this limit, catalytic interactions dominate over triple-wave interactions, which is the case in figure 13(*b*).

The total vortical energy transfer is approximately zero between the forcing at $k_z=0$ and the dissipation, implying a well-resolved inertial range (figure 13*c*, *d*). When $N=4$ (figure 13*c*), the downscale transfer of vortical energy is dominated by $(0,\pm,0)$ and $(0,0,0)$ interactions. When $N=16$ (figure 13*d*), the $(0,\pm,0)$ contribution is greatly reduced, and the transfer of vortical energy to small vertical scales is dominated by interactions involving three vortical modes, which trivially meet the resonance condition. The vortical side of the catalytic interaction involving two wave modes and a vortical mode is nearly zero everywhere when $N=16$, as required by the conservation of the quadratic potential enstrophy V.

https://doi.org/10.1017/S0022112004000977 Published online by Cambridge University Press

4.3.4. *Vertical length scales*

The vortical and wave energy spectra have characteristic vertical length scales, which can be compared to the scale U/N predicted by Billant & Chomaz (2001). We define U in terms of the time-averaged vortical energy (which dominates the total energy) as in (4.11). The vortical energy spectra of our simulations are flat out to a wavenumber which we denote by k_c, and can be modelled by

$$E_z^{(0)}(k_z) = \begin{cases} a, & k_z \leqslant k_c \\ a(k_z/k_c)^{-p}, & k_z > k_c, \end{cases} \tag{4.17}$$

where $p > 1$ and, integrating over k_z,

$$a = \left(\frac{p-1}{pk_c}\right) E^{(0)}. \tag{4.18}$$

The vortical scale is $1/k_c$, and is the vertical length over which velocities are correlated.

It is easy to show that $k_c \sim N/U$. The spectral Froude number at k_z is

$$Fr_z(k_z) \equiv \frac{U(k_z)k_z}{N} = \frac{\sqrt{2a}k_z^{3/2}}{N}, \tag{4.19}$$

in the flat range, where

$$U(k_z) = \left(\int_0^{k_z} 2E_z^{(0)}(s)\,\mathrm{d}s\right)^{1/2}. \tag{4.20}$$

Assuming that overturning destroys the vertical decoupling of the flat range, it follows that $Fr_z(k_c) \sim 1$. Using (4.18) to eliminate a in (4.19), we have

$$k_c \sim \left(\frac{p}{p-1}\right)^{1/2} \frac{N}{\sqrt{2E^{(0)}}} = \left(\frac{p}{p-1}\right)^{1/2} \frac{N}{U}. \tag{4.21}$$

The end of the flat range therefore occurs near N/U.

As a means of measuring k_c in our spectra, consider the nth moment of $E_z^{(0)}(k_z)$,

$$\overline{k}_z^{(n)} = \left(\frac{\int k_z^n E_z^{(0)}(k_z)\,\mathrm{d}k_z}{\int E_z^{(0)}(k_z)\,\mathrm{d}k_z}\right)^{1/n}. \tag{4.22}$$

Letting $Re \to \infty$ and integrating between 0 and ∞ in (4.22), the spectrum (4.17) gives

$$\overline{k}_z^{(n)} = \left(\frac{p-1}{(n+1)(p-n-1)}\right)^{1/n} k_c, \tag{4.23}$$

provided that $n < p-1$. The usual choice of $n = 1$ is invalid if we are to allow for the possibility that $p = 5/3$. Instead, we choose (somewhat arbitrarily) $n = 1/2$, which explains our definition of $\overline{k}_z$ in (4.10). We have defined $\overline{k}_h$ analogously.

The wave field introduces two characteristic vertical wavenumbers, corresponding to the maximum wave energy $E_z^{(\pm)}(k_z)$ and the maximum wave/vortical exchange $T_z^{(\pm,0,0)}(k_z)$, which we call k_w and k_e, respectively. We have computed k_w and k_e, with finite difference and linear interpolation, after first smoothing the energy and transfer spectra with a three-point running average (applied once for the energy spectra, and between three and five times for the transfer spectra). Both k_w and k_e are plotted against Fr_h in figure 14. In most cases, k_e exceeds k_w by about a factor of two. As we

https://doi.org/10.1017/S0022112004000977 Published online by Cambridge University Press

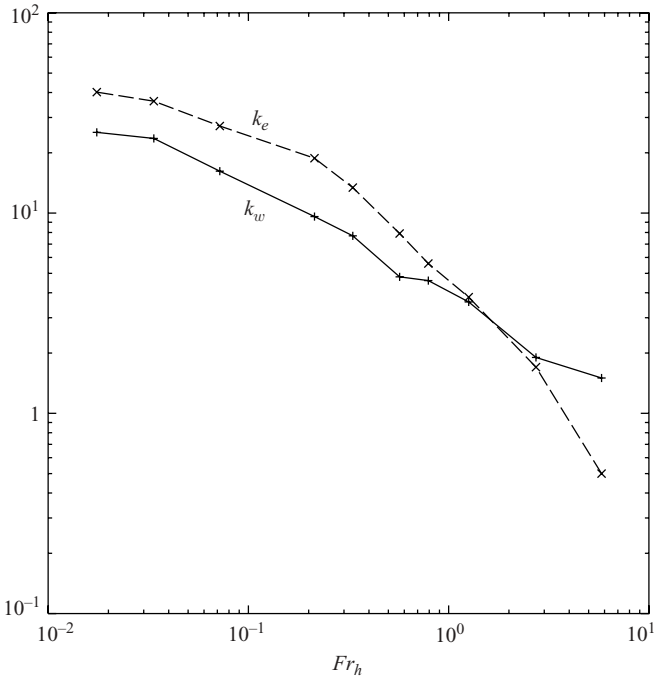


FIGURE 14. The vertical wavenumber of maximum wave energy $E_z^{(\pm)}$ (k_w) and maximum wave/vortical exchange $T_z^{(\pm,0,0)}$ (k_e) plotted against Fr_h.

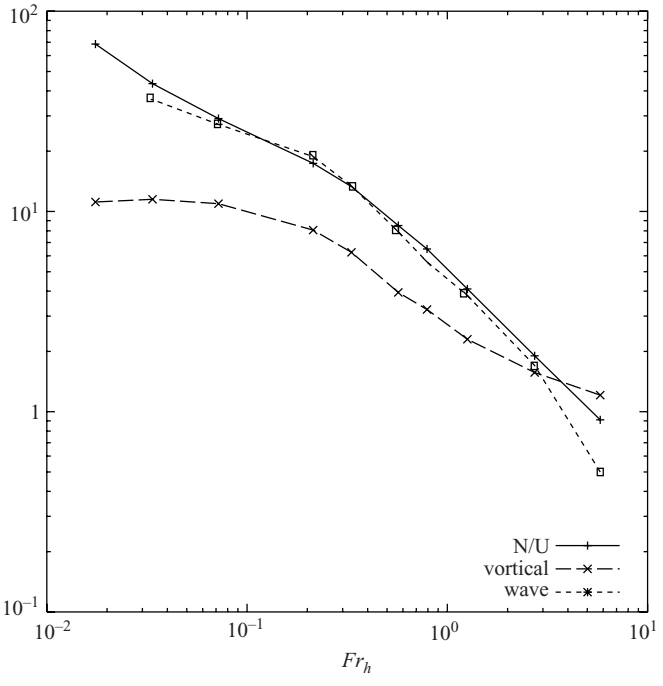


FIGURE 15. N/U along with the characteristic wavenumbers $\overline{k}_z$ (vortical) and k_e (wave), as functions of Fr_h

https://doi.org/10.1017/S0022112004000977 Published online by Cambridge University Press

saw in figure 13, wave energy is injected at $k_z \sim k_e$ and swept downscale and dissipated (by small-scale turbulence when Re is large enough). This process is responsible for the dissipation of large-scale vortical energy, and its vertical scale is the scale at which the layered structure of stratified turbulence breaks down. We anticipate that k_e should scale like $\overline{k}_z$ and U/N.

The vortical wavenumber $\overline{k}_z$, the wave wavenumber k_e, and N/U are plotted together against Fr_h in figure 15. The wavenumber $\overline{k}_z$ scales approximately like N/U for $0.2 < Fr_h < 1$; it is limited by the dissipation scale at small Fr_h and the domain size at large Fr_h. The wavenumber k_e agrees well with N/U over a slightly wider range than $\overline{k}_z$, probably because the wave energy is not directly contaminated by the forcing. In addition, we have computed the buoyancy wavenumber k_b for each of our runs, using the total dissipation rate $\epsilon = \epsilon_h^{(0)} + \epsilon_h^{(\pm)} + \epsilon_z^{(0)} + \epsilon_z^{(\pm)}$ as defined in (4.14); k_b values are given in table 1. In most instances k_b is much larger than N/U and k_d; indeed, only when $N \leqslant 1$ is $k_b < k_d$. Higher resolution is required to resolve both N/U and k_b when the stratification is strong. Nevertheless, our primary interest is in the scale of the breakdown of the layered structure of stratified turbulence, which appears to scale convincingly as U/N. The nature of the buoyancy range at wavenumbers larger than N/U, and the transition to isotropy at k_b, cannot be clearly determined from these results.

5. Conclusions

We have presented a set of simulations of forced turbulence at various stratifications. Our aim was to study the dynamics of turbulence dominated by the vortical component of the flow. Large-scale vortical motion was forced for many turnover times, until statistical stationarity was reached. A small amount of initial seed energy guaranteed that vertical structure would emerge, and with it, internal waves and (in most instances) overturning. Ten stratifications were considered, covering a wide range of Froude numbers. Our weakest stratification had horizontal Froude number $Fr_h = 6$, while our two strongest stratifications suppressed all overturning. As in other recent studies of forced stratified turbulence (Smith & Waleffe 2002; Laval *et al.* 2003), we observed a slow growth in the kinetic energy of the horizontally averaged velocity. The growth rate dropped rapidly in the strongly stratified limit when all overturning was suppressed.

The main results of our forced–dissipative simulations can be summarized as follows. For weak stratification, the vertical spectra of vortical energy resemble $k_z^{-5/3}$. As the stratification is increased, a flat range emerges at low wavenumbers. The flat range is a consequence of the vertical decoupling, and its length was shown to scale as N/U, the characteristic scale of Billant & Chomaz (2001). Overturning motion accounts for the non-zero slope beyond, which appears to steepen as N increases. However, the details of the steepening are unclear at this resolution. Higher resolution is necessary to simultaneously resolve the large decoupled scales and the small isotropic scales, and to determine the length of any intermediate range with a non-zero slope distinct from $-5/3$. On increasing N, the negative slope range moves out towards k_d and narrows, eventually disappearing as all overturning is suppressed. In this limit, the vertical spectrum is flat out to the dissipation range, and the layers are coupled only by viscosity. In the horizontal, the vortical spectra are slightly shallower than $k_h^{-5/3}$ at low and moderate stratifications, consistent with the results of Riley & deBruynKops (2003) and Lindborg (2003, personal communication). They steepen as N increases, saturating with a slope of approximately -5 in the absence of overturning, as in Laval

https://doi.org/10.1017/S0022112004000977 Published online by Cambridge University Press

et al. (2003). The limiting vortical spectra, i.e. flat in k_z and with a slope near -5 in k_h, agree well with those obtained by integrating directly the reduced equations for vortical motion. The inhibited transfer to small horizontal scales and efficient transfer to small vertical scales were suggested by the statistical mechanical equilibrium, which also confirms the absence of an inverse energy cascade in stratified turbulence.

Wave energy was not forced directly, but was generated through nonlinear interactions with the vortical motion. In all but the most strongly stratified cases, wave energy is injected at a vertical scale of U/N. At this scale, $Fr_z \sim O(1)$, and so one must be cautious in interpreting the injected wave energy; it may correspond to strongly nonlinear stratified turbulence, rather than internal waves satisfying the dispersion relation (2.2). The spectra of wave energy have positive slope out to this scale, as in Laval *et al.* (2003). As stratification increases, the spectral peak of wave energy moves out to large k_z and small k_h, where low-frequency wave modes are located. The triadic interaction of one wave mode and two vortical modes, which is responsible for the injection of wave energy, is the least off-resonant in this region of the k_h–k_z plane.

The end of the flat range and the injection of wave energy occur at a vertical scale which scales like U/N, agreeing with the prediction of Billant & Chomaz (2001). In fact, U/N is the scale at which vortical motion breaks down into overturning three-dimensional motion. For $k_z \ll N/U$, the spectral Froude number $Fr_z(k_z) \ll 1$ and layers of horizontal flow are decoupled from one another, as described by the reduced equations. At scales near U/N, $Fr_z \sim O(1)$ and overturning occurs, while buoyancy effects are still important. The buoyancy wavenumber k_b also introduces an important scale, below which stratification is unimportant and isotropic three-dimensional turbulence exists. This scale was unresolved in most of our simulations.

The spectra obtained in the limit of strong stratification, despite agreeing with the reduced equations, look nothing like the standard observations in the atmosphere and ocean. More interesting is the nature of the turbulence below the overturning scale, about which many questions remain. How wide is the range of length scales between U/N and the eventual transition to isotropy? How does the turbulence in this range compare with that generated by breaking internal waves? The wave/vortical decomposition loses its usefulness below the overturning scale, and so it may be more fruitful to focus on kinetic and potential energy and the buoyancy flux, as in Ramsden & Holloway (1992). The effects of weak rotation and spatial inhomogeneity, which are present in the real atmosphere and ocean, should also be examined.

The authors would like to thank K. Ngan and D. N. Straub for helpful discussions, as well as P. Billant, C. Cambon, G. Holloway, E. Lindborg, J. J. Riley, L. M. Smith, C. Staquet, F. Waleffe and K. Yoshida for thoughtful comments on the manuscript. Support from the National Science and Engineering Research Council of Canada and the Meteorological Service of Canada (MSC) is also gratefully acknowledged. Computer time was provided by MSC and the Consortium Laval–UQAM–McGill et l'Est du Québec.

REFERENCES

Asselin, R. 1972 Frequency filter for time integrations. *Mon. Wea. Rev.* **100**, 487–490.

Babin, A., Mahalov, A., Nicolaenko, B. & Zhou, Y. 1997 On the asymptotic regimes and the strongly stratified limit of rotating Boussinesq equations. *Theor. Comput. Fluid Dyn.* **9**, 223–251.

https://doi.org/10.1017/S0022112004000977 Published online by Cambridge University Press

Bacmeister, J. T., Eckermann, S. D., Newman, P. A., Lait, L., Chan, K. R., Lowenstein, M., Proffitt, M. H. & Gary, B. L. 1996 Stratospheric horizontal wavenumber spectra of winds, potential temperature, and atmospheric tracers observed by high-altitude aircraft. *J. Geophys. Res.* **101**, 9441–9470.

Bartello, P. 1995 Geostrophic adjustment and inverse cascades in rotating stratified turbulence. *J. Atmos. Sci.* **52**, 4410–4428.

Bartello, P., Métais, O. & Lesieur, M. 1996 Geostrophic versus wave eddy viscosities in atmospheric models. *J. Atmos. Sci.* **53**, 564–571.

Billant, P. & Chomaz, J.-M. 2000 Experimental evidence for a new instability of a vertical columnar vortex pair in a strongly stratified fluid. *J. Fluid Mech.* **418**, 167–188.

Billant, P. & Chomaz, J.-M. 2001 Self-similarity of strongly stratified inviscid flows. *Phys. Fluids* **13**, 1645–1651.

Bolgiano Jr, R. 1959 Turbulence spectra in a stably stratified atmosphere. *J. Geophys. Res.* **64**, 2226–2229.

Bouruet-Aubertot, P., Sommeria, J. & Staquet, C. 1996 Stratified turbulence produced by internal wave breaking: Two-dimensional numerical experiments. *Dyn. Atmos. Oceans* **23**, 357–369.

Caillol, P. & Zeitlin, V. 2000 Kinetic equations and stationary energy spectra of weakly nonlinear internal gravity waves. *Dyn. Atmos. Oceans* **32**, 81–112.

Carnevale, G. F., Briscolini, M. & Orlandi, P. 2001 Buoyancy- to inertial-range transition in forced stratified turbulence. *J. Fluid Mech.* **427**, 205–239.

Cho, J. Y. N., Newell, R. E. & Barrick, J. D. 1999 Horizontal wavenumber spectra of winds, temperature, and trace gases during the Pacific exploratory missions: 2. Gravity waves, quasi-two-dimensional turbulence, and vortical modes. *J. Geophys. Res.* **104**, 16297–16308.

Dewan, E. M. 1979 Stratospheric wave spectra resembling turbulence. *Science* **204**, 832–835.

Dewan, E. M. & Good, R. E. 1986 Saturation and the 'universal' spectrum for vertical profiles of horizontal scalar winds in the atmosphere. *J. Geophys. Res.* **91**, 2742–2748.

Embid, P. F. & Majda, A. J. 1998 Low Froude number limiting dynamics for stably stratified flow with small or finite Rossby numbers. *Geophys. Astrophys. Fluid Dyn.* **87**, 1–50.

Fincham, A. M., Maxworthy, T. & Spedding, G. R. 1996 Energy dissipation and vortex structure in freely decaying, stratified grid turbulence. *Dyn. Atmos. Oceans* **23**, 155–169.

Gage, K. S. 1979 Evidence for a $k^{-5/3}$ law inertial range in mesoscale two-dimensional turbulence. *J. Atmos. Sci.* **36**, 1950–1954.

Gargett, A. E., Hendricks, P. J., Sanford, T. B., Osborn, T. R. & Williams, A. J. 1981 A composite spectrum of vertical shear in the upper ocean. *J. Phys. Oceanogr.* **11**, 1258–1271.

Gargett, A. E., Osborn, T. R. & Nasmyth, P. W. 1984 Local isotropy and the decay of turbulence in a stratified fluid. *J. Fluid Mech.* **144**, 231–280.

Godeferd, F. S. & Cambon, C. 1994 Detailed investigation of energy transfers in homogeneous stratified turbulence. *Phys. Fluids* **6**, 2084–2100.

Godeferd, F. S. & Staquet, C. 2003 Statistical modelling and direct numerical simulations of decaying stably stratified turbulence. Part 2. Large-scale and small-scale anisotropy. *J. Fluid Mech.* **486**, 115–159.

Herring, J. R. 1974 Approach of axisymmetric turbulence to isotropy. *Phys. Fluids* **17**, 859–872.

Herring, J. R. & Métais, O. 1989 Numerical experiments in forced stably stratified turbulence. *J. Fluid Mech.* **202**, 97–115.

Hines, C. O. 1996 Nonlinearity of gravity wave saturated spectra in the middle atmosphere. *Geophys. Res. Lett.* **23**, 3309–3312.

Holloway, G. 1986 Eddies, waves, circulation, and mixing: Statistical geofluid mechanics. *Annu. Rev. Fluid Mech.* **18**, 91–147.

Hopfinger, E. J. 1987 Turbulence in stratified fluids: A review. *J. Geophys. Res.* **92**, 5287–5303.

Kimura, Y. & Herring, J. R. 1996 Diffusion in stably stratified turbulence. *J. Fluid Mech.* **328**, 253–269.

Kolmogorov, A. N. 1941 The local structure of turbulence in incompressible viscous fluid for very large Reynolds number. *Dok. Akad. Nauk. SSSR* **30**, 301–305.

Kraichnan, R. H. 1967 Inertial ranges in two-dimensional turbulence. *Phys. Fluids* **10**, 1417–1423.

Kraichnan, R. H. 1975 Statistical dynamics of two-dimensional flow. *J. Fluid Mech.* **67**, 155–175.

Laval, J.-P., McWilliams, J. C. & Dubrulle, B. 2003 Forced stratified turbulence: Successive transitions with Reynolds number. *Phys. Rev.* E **68**, 036308.

https://doi.org/10.1017/S0022112004000977 Published online by Cambridge University Press

Lee, T. 1952 On some statistical properties of hydrodynamical and magneto-hydrodynamical fields. *Q. Appl. Maths* **10**, 69–78.

Lelong, M.-P. & Riley, J. J. 1991 Internal wave-vortical mode interactions in strongly stratified flows. *J. Fluid Mech.* **232**, 1–19.

Lesieur, M. 1997 *Turbulence in Fluids*, 3rd edn. Kluwer.

Lilly, D. K. 1983 Stratified turbulence and the mesoscale variability of the atmosphere. *J. Atmos. Sci.* **40**, 749–761.

Lumley, J. L. 1964 The spectrum of nearly inertial turbulence in a stably stratified fluid. *J. Atmos. Sci.* **21**, 99–102.

McComas, C. H. & Müller, P. 1981 The dynamic balance of internal waves. *J. Phys. Oceanogr* **11**, 970–986.

Métais, O., Bartello, P., Garnier, E., Riley, J. J. & Lesieur, M. 1996 Inverse cascade in stably stratified rotating turbulence. *Dyn. Atmos. Oceans* **23**, 193–203.

Métais, O. & Lesieur, M. 1992 Spectral large-eddy simulation of isotropic and stably stratified turbulence. *J. Fluid Mech.* **239**, 157–194.

Müller, P., Holloway, G., Henyey, F. & Pomphrey, N. 1986 Nonlinear interactions among internal gravity waves. *Rev. Geophys.* **24**, 493–536.

Munk, W. 1981 Internal waves and small-scale processes. In *Evolution of Physical Oceanography* (ed. B. A. Warren & C. Wunsch), pp. 264–291. MIT Press.

Nastrom, G. D. & Gage, K. S. 1985 A climatology of atmospheric wavenumber spectra observed by commercial aircraft. *J. Atmos. Sci.* **42**, 950–960.

Nastrom, G. D., Van Zandt, T. E. & Warnock, J. M. 1997 Vertical wavenumber spectra of wind and temperature from high-resolution balloon soundings over Illinois. *J. Geophys. Res.* **102**, 6685–6701.

Pedlosky, J. 1987 *Geophysical Fluid Dynamics*, 2nd edn. Springer.

Polzin, K. L., Kunze, E., Toole, J. M. & Schmitt, R. W. 2003 The partition of finescale energy into internal waves and subinertial motions. *J. Phys. Oceanogr.* **33**, 234–248.

Ramsden, D. & Holloway, G. 1992 Energy transfers across an internal wave-vortical mode spectrum. *J. Geophys. Res.* **97**, 3659–3668.

Riley, J. J. & deBruynKops, S. M. 2003 Dynamics of turbulence strongly influenced by buoyancy. *Phys. Fluids* **15**, 2047–2059.

Riley, J. J. & Lelong, M.-P. 2000 Fluid motions in the presence of strong stable stratification. *Annu. Rev. Fluid Mech.* **32**, 613–657.

Riley, J. J., Metcalfe, R. W. & Weissman, M. A. 1981 Direct numerical simulations of homogeneous turbulence in density-stratified fluids. In *Nonlinear Properties of Internal Waves* (ed. B. J. West), pp. 79–112. AIP.

Smith, L. M. & Waleffe, F. 2002 Generation of slow large scales in forced rotating stratified turbulence. *J. Fluid Mech.* **451**, 145–168.

Smith, S. A., Fritts, D. C. & Van Zandt, T. E. 1987 Evidence for a saturated spectrum of atmospheric gravity waves. *J. Atmos. Sci.* **44**, 1404–1410.

Staquet, C. & Riley, J. J. 1989 On the velocity field associated with potential vorticity. *Dyn. Atmos. Ocean* **14**, 93–123.

Thoroddsen, S. T. & Atta, C. W. V. 1992 The influence of stable stratification on small-scale anisotropy and dissipation in turbulence. *J. Geophys. Res.* **97**, 3647–3658.

Van Zandt, T. E. 1982 A universal spectrum of buoyancy waves in the atmosphere. *Geophys. Res. Lett.* **9**, 575–578.

Warn, T. 1986 Statistical mechanical equilibria of the shallow water equations. *Tellus* **38A**, 1–11.

https://doi.org/10.1017/S0022112004000977 Published online by Cambridge University Press